US005963662A

United States Patent [19]

Vachtsevanos et al.

[11] Patent Number: 5,963,662

[45] Date of Patent: *Oct. 5, 1999

[54] **INSPECTION SYSTEM AND METHOD FOR BOND DETECTION AND VALIDATION OF SURFACE MOUNT DEVICES**

[75] Inventors: **George J. Vachtsevanos**, Marietta; **Iqbal M. Dar**, Atlanta; **Kimberly E. Newman**, Atlanta; **Erin Sahinci**, Atlanta, all of Ga.

[73] Assignee: **Georgia Tech Research Corporation**, Atlanta, Ga.

[*] Notice: This patent issued on a continued prosecution application filed under 37 CFR 1.53(d), and is subject to the twenty year patent term provisions of 35 U.S.C. 154(a)(2).

[21] Appl. No.: **08/753,181**

[22] Filed: **Nov. 20, 1996**

Related U.S. Application Data

[60] Provisional application No. 60/023,519, Aug. 7, 1996.

[51] **Int. Cl.**[6] **G01N 25/72**; G01N 21/71; G06T 5/20

[52] **U.S. Cl.** **382/150**; 382/146; 382/147; 374/10; 250/332

[58] **Field of Search** 382/145, 147, 382/148, 149, 150; 348/164, 87, 126, 131, 166, 165; 356/51, 372, 237; 364/468.17, 557; 324/451, 501; 438/15, 16; 374/5, 10; 228/103, 105; 209/577; 250/330, 316.1, 332, 339.02, 339.14, 341.1, 341.6, 342; 29/407.04

[56] **References Cited**

U.S. PATENT DOCUMENTS

3,795,918	3/1974	Sunderland	356/45
5,115,475	5/1992	Lebeau	382/146

FOREIGN PATENT DOCUMENTS

2257508	1/1993	United Kingdom	G01J 5/10

OTHER PUBLICATIONS

G. Hamid, An FPGA–Based CoproCessor For Image Processing, IEEE/IEE Publication, 1994, pp. 6/1–6/4.

Jonathan Rose et al., Architecture of Field–Programmable Gate Arays: The Effect of Logic Block Functionality on Area Efficiency, IEEE Publication, 1990, pp. 1217–1225.

Dennis Lazaroff et al., Evaluating Different Sampling Technique for Process Control Using Automated Patterened Wafer Inspection Systems, IEEE Publication, 1991, pp. 92–97.

Roger Z. Liu et al., Infrared Solder Joint Inspection on Surface Mount Printed Circuit Boards, IEEE Publication, Apr. 1996 pp. 145–148.

L. Zadeh, "Fuzzy Sets as a Basis for a Theory of Poss.", Fuzzy Sets and Sys., Dept. of Electrical Engineering & Sciences, Univ. of Cal., Berkeley, CA., vol. 1, pp. 3–28, 1978.

(List continued on next page.)

Primary Examiner—Leo H. Boudreau
Assistant Examiner—Brian P. Werner
Attorney, Agent, or Firm—Thomas, Kayden, Horstemeyer & Risley

[57] **ABSTRACT**

A hybrid surface mount component inspection system which includes both vision and infrared inspection techniques to determine the presence of surface mount components on a printed wiring board, and the quality of solder joints of surface mount components on printed wiring boards by using data level sensor fusion to combine data from two infrared sensors to obtain emissivity independent thermal signatures of solder joints, and using feature level sensor fusion with active perception to assemble and process inspection information from any number of sensors to determine characteristic feature sets of different defect classes to classify solder defects.

18 Claims, 27 Drawing Sheets
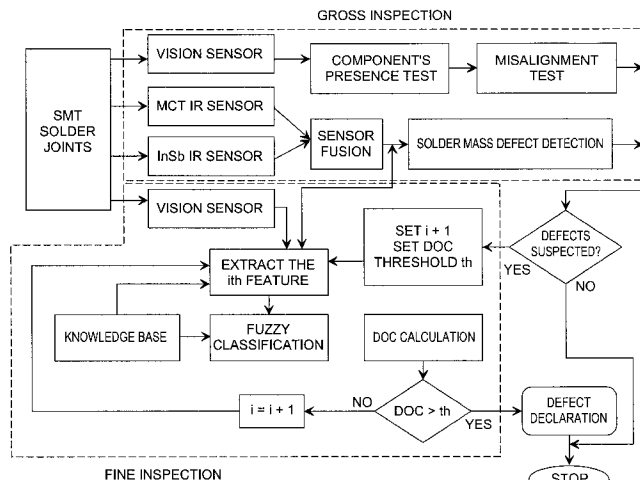
OTHER PUBLICATIONS

D.W. Capson et al., "A Tiered Color Illum. Approach for Machine Inspec. Of Solder Joints", IEEE Trans. on Patt. Anal. Machine Intell., vol. PAM1–10, pp. 387–393, May 1988.

S.L. Bartlett et al., "Automatic Solder Joint Inspec.", IEEE Trans. on Pattern Anal. Machine Intell., vol. PAM1–10, pp. 31–42, Jan. 1988.

Riccardo Vanzetti et al., "Combining Soldering with Inspection", IEEE Control Sys. Mag., pp. 29–31, Oct. 1988.

M. Juha, "X–ray Machine Vision for Circuit Brd. Inspec." Proceedings of Vision 86 Conf. of SME, Detroit, Michigan pp. 3–41–3–55, Jun. 1986.

Kenneth Reid, "Automated Soldering Inspection Technology Study", Proceedings of Tech. Program of NEPCON West, Anaheim, Cal., vol. 3, pp. 1288–1297, Feb., 1993.

I, Dar et al., "Bond Validation of Surface Mount Comp. Using Combined IR/Vision Sys.", App. Machine Vision 94 Conf. of SME, Minn., vol. 2, session 7, Jun., 1994.

Lofti A. Zadeh, "Outline of a New Approach . . . Sys. and Decision Processes", IEEE Trans. on Sys. Mann., Cybern, vol. SMC–3, No. 1, pp. 28–44, 1973.
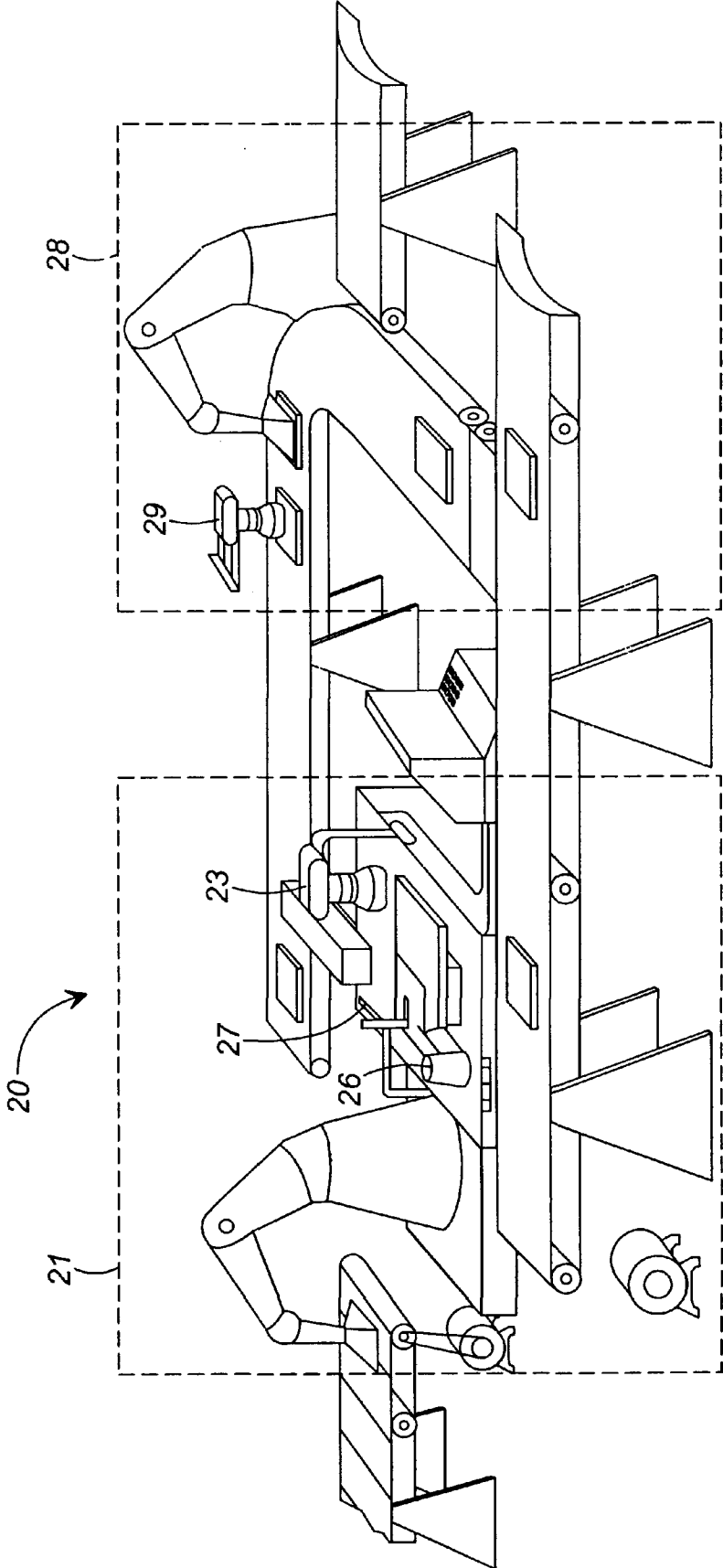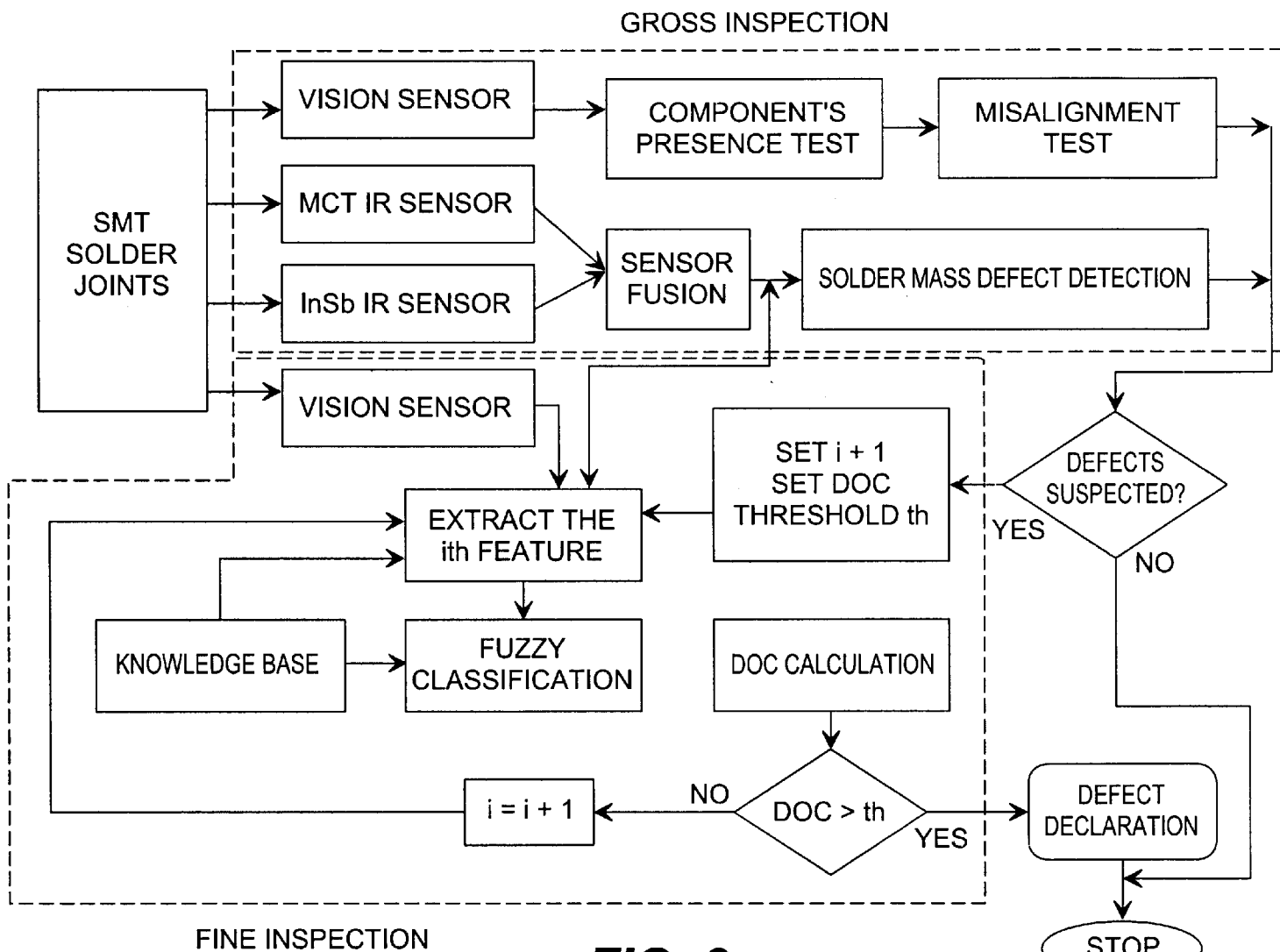
FIG. 1

GROSS INSPECTION

FIG. 2

SMT SOLDER JOINTS

VISION SENSOR

COMPONENT'S PRESENCE TEST

MISALIGNMENT TEST

MCT IR SENSOR

InSb IR SENSOR

SENSOR FUSION

SOLDER MASS DEFECT DETECTION

VISION SENSOR

SET i + 1 SET DOC THRESHOLD th

DEFECTS SUSPECTED?

YES

NO

EXTRACT THE ith FEATURE

KNOWLEDGE BASE

FUZZY CLASSIFICATION

DOC CALCULATION

i = i + 1

NO

DOC > th

YES

DEFECT DECLARATION

STOP

FINE INSPECTION

FIG. 3

30

┌───┐
│ CAPTURE IMAGE USING   │
│ OBLIQUE ILLUMINATION   │
└───┘

32

34

COMPONENT
PRESENT?   NO →

YES

36

┌───┐
│ CAPTURE IMAGE USING   │
│ A FLAT ILLUMINATION   │
└───┘

VISION

38

┌───┐
│ LINEAR MISALIGNMENT   │
│ TEST   │
└───┘

42

┌───┐
│ ANGULAR MISALIGNMENT   │
│ TEST   │
└───┘

┌───┐
│ CAPTURE THERMAL   │
│ SIGNATURE   │
└───┘

INFRARED

DEFECTIVE
BONDS?   YES →

NO

STOP

FIG. 4

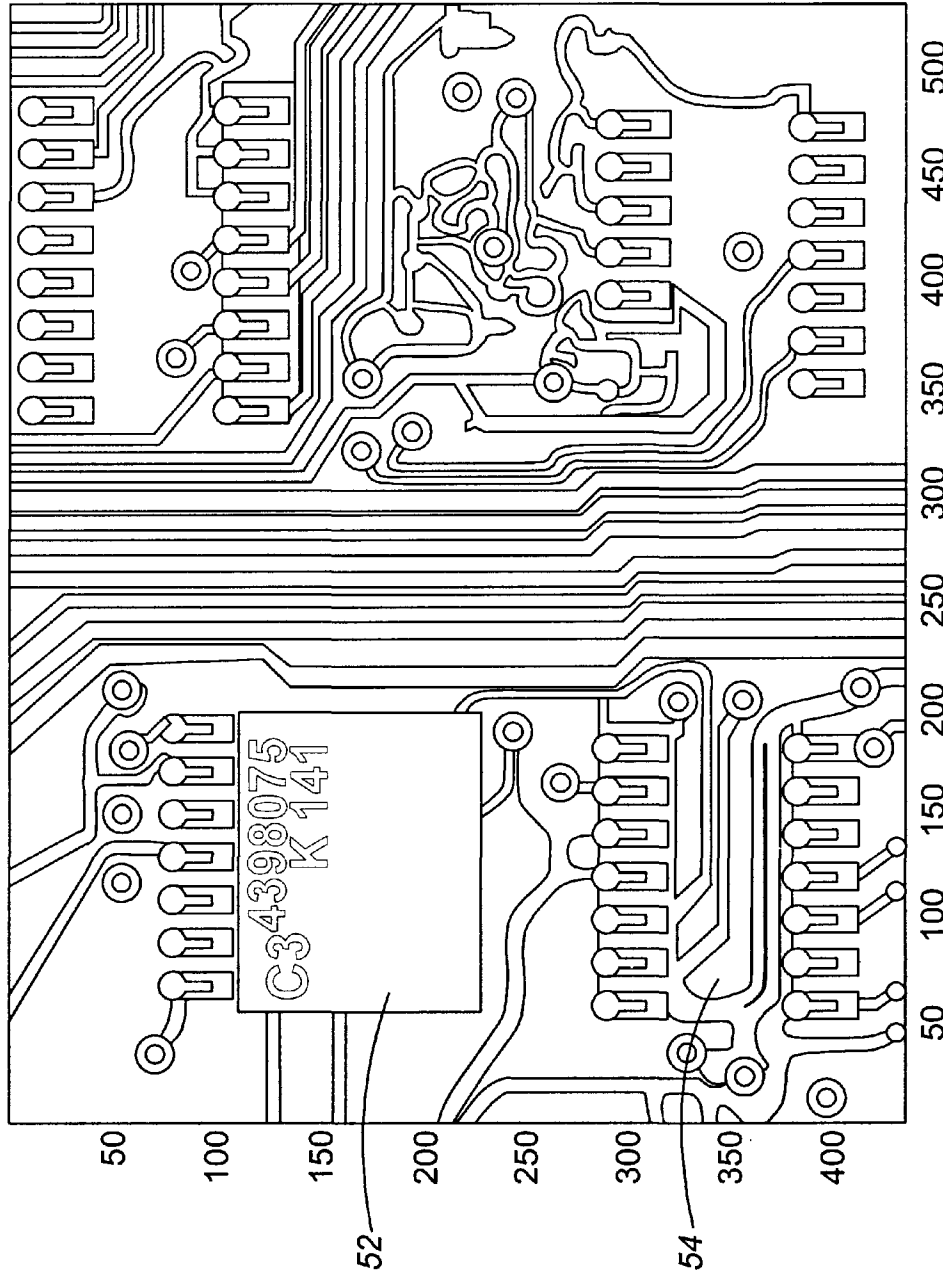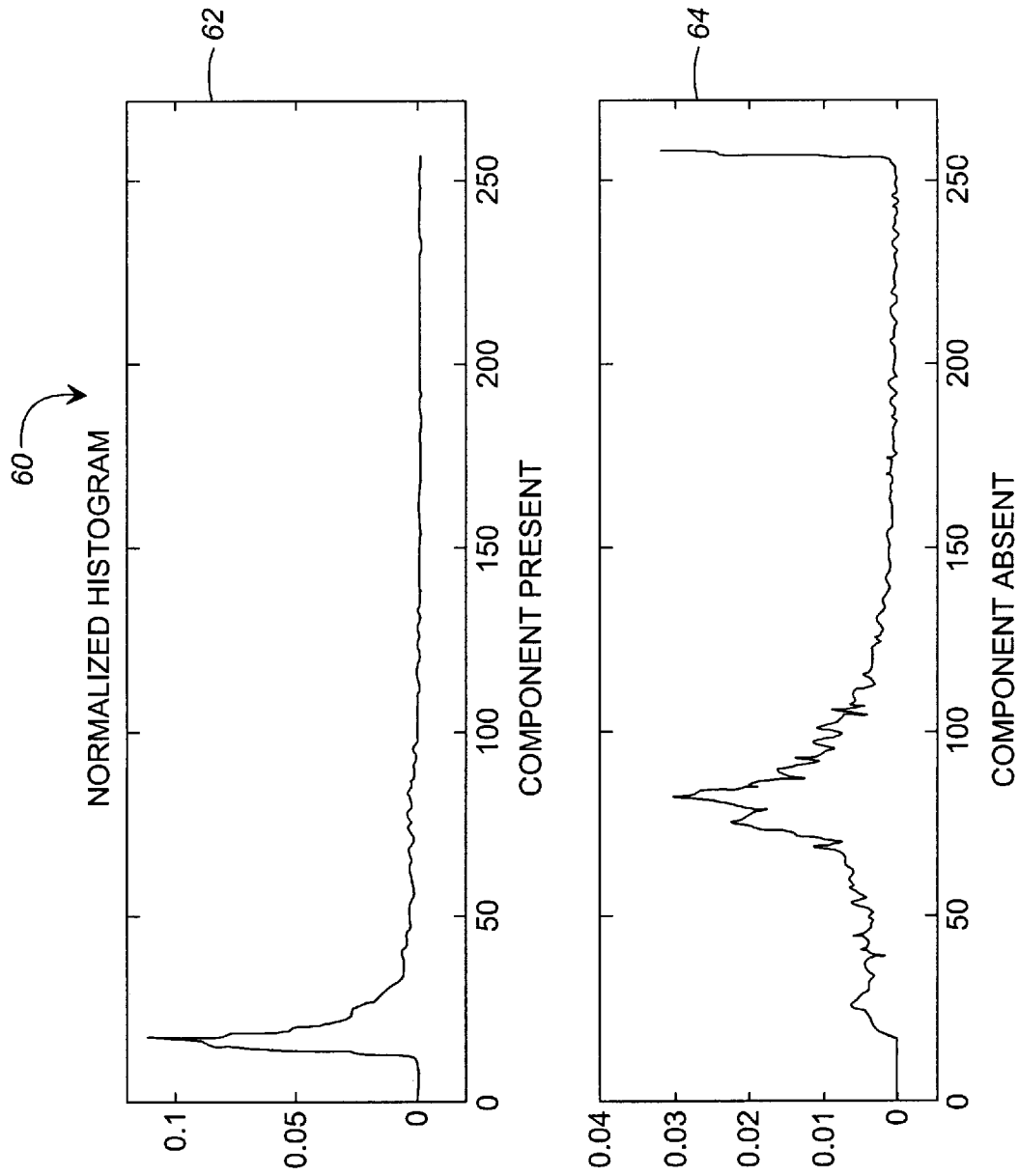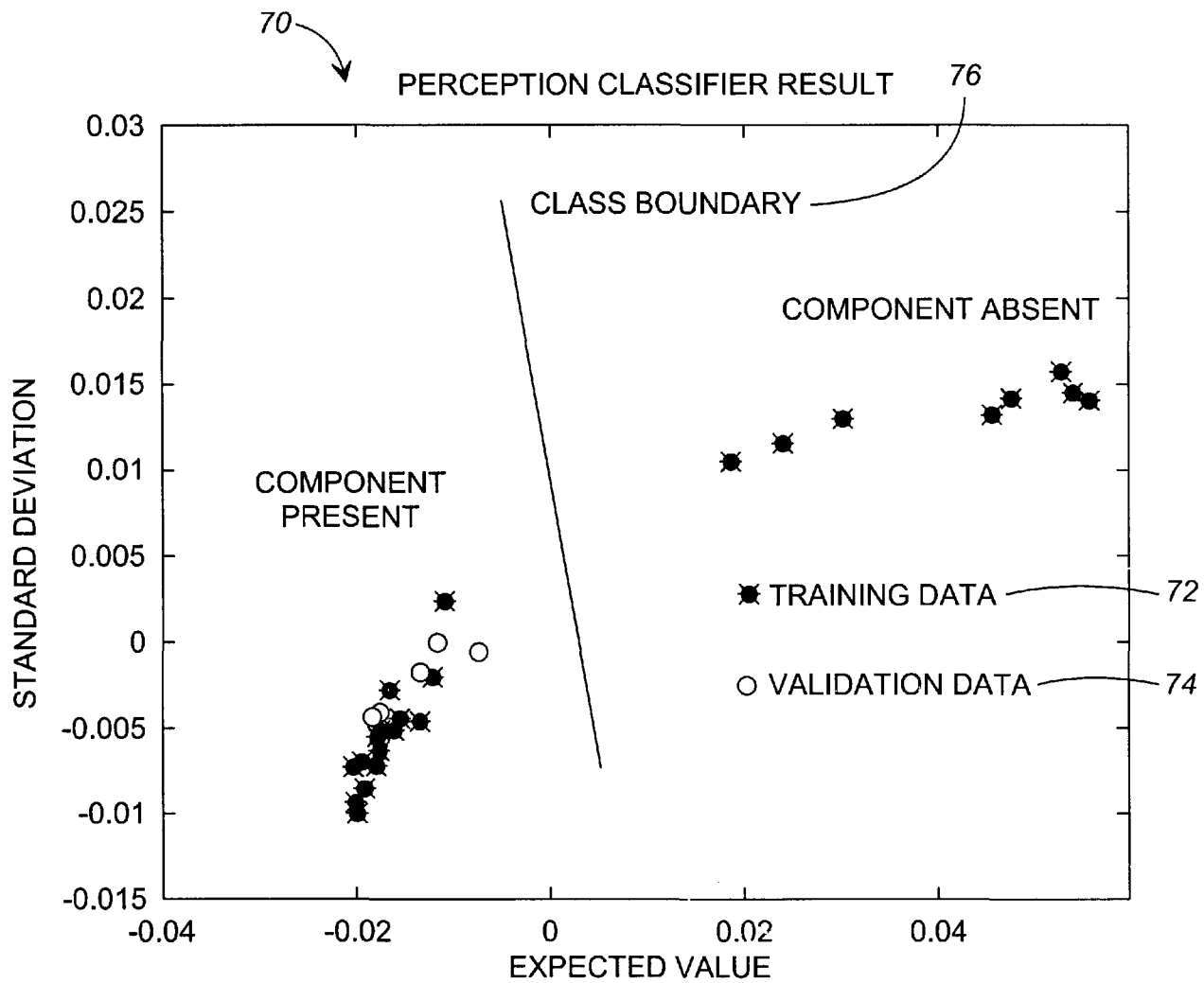*FIG. 5*

FIG. 6

FIG. 7

FIG. 8

FIG. 9

FIG. 10

92,A   SOLDER PADS   B,94

A,B,C, AND D
ARE OUTSIDE CORNERS

LEADS

D,98

C,96

FIG. 11

101   91   99

97   93

VERY
NEGATIVE   NEGATIVE   ZERO   POSITIVE   VERY
POSITIVE

1

0

UNIVERSE OF DISCOURSE

FIG. 12

FIG. 13

FIG. 14

118 INSO SENSOR

MGT SENSOR

119

100

80

60

40

20

0

% TRANSMITTANCE

0.007

0.006

0.005

0.004

0.003

0.002

0.001

Rn TIMER - - - →

116

114

112

75°C

50°C

25°C

1.5 3.0 4.5 6.0 7.5 9.0 10.5 12.0 3.5

WAVELENGTH   MICRONS

FIG. 15

MCT DETECTOR OUTPUT

InSB DETECTOR OUTPUT

111

Z SIGNAL

FIG. 16

DATA BASE

PLUS-MARKED	– – →	INSUFFICIENT
×-MARKED	– – – →	NO SOLDER
SOLID	– – – – →	GOOD
DOTTED	– – – – →	BALL
DASHDOTTED	– – →	EXCESSIVE
DASHED	– – – – →	BRIDGING

117

113

119

FIG. 17

GROSS FILTER FEATURES

122

GOOD
JOINTS

INSUFFICIENT SOLDER DEFECTS

EXCESS SOLDER
DEFECTS

124

MAX VALUE MINUS THE END POINT

MAX VALUE MINUS THE STARTING POINT

FIG. 18

132 DATA ACQUISITION   PREPROCESSING *138*

134 → VISION SENSOR → IMAGE PROCESSING ~ *137*

SOLDER JOINTS

IR SENSOR → THERMAL PROCESSING ~ *139*

136

GROSS FILTER   GROSS FILTER   GROSS FILTER

144   *146*

142 LINEAR MISALIGNMENT TEST   INSUFFICIENT SOLDER MASS TEST   EXCESS SOLDER MASS TEST

FIG. 19

DEFECT DECLARATION

GOOD SOLDER JOINTS

LINEAR MISALIGNMENT

151

SOLDER BALL

EXCESS SOLDER

BRIDGING

INSUFFICIENT SOLDER

FIG. 20

FIG. 21

162 — FUZZY CLASS MEMBERSHIP

164 — CALCULATE POSSIBILITY DISTRIBUTION

166 — CALCULATE MASS FUNCTION

168 — CALCULATE DOC

STOP

FIG. 22

FIG. 23

170

```
        ┌──────────────┐
        │  SET i = 1   │
        │  SET DOC     │
        │ THRESHOLD th │
        └──────┬───────┘
               │
               ▼
          ╱─────────────╲        YES
         ╱  i > TOTAL    ╲──────────────┐
         ╲  FEATURES     ╱              │
          ╲─────────────╱               │
               │ NO                     │
               ▼                        │
         176                            │
         ┌──────────────────┐           │
  174    │ EXTRACT ith      │           │
         │ FEATURE          │           │
  171    └────────┬─────────┘           │
         SENSOR 1          178          │
         SENSOR 2  ┌──────────────────┐ │
            ⋮      │ FUZZY            │ │
         SENSOR N  │ CLASSIFICATION   │ │
                   └────────┬─────────┘ │
  172                    173            │
  ┌───────────┐   ┌──────────────────┐  │
  │ KNOWLEDGE │   │ CALCULATE DOC    │  │
  │ BASE      │   └────────┬─────────┘  │
  └───────────┘            │            │
                           ▼            │
   ┌───────┐   NO     ╱─────────╲  YES  ▼
   │i = i+1│◄─────────╲ DOC>=th ╱─────► (STOP)
   └───────┘           ╲───────╱
                         177
```

FIG. 24

184

$P_1(z)$

$P_2(z)$

T

1   −182   2

FIG. 25

MEAN VALUE OF A FEATURE
FOR A PARTICULAR CLASS

192

SIX TIMES THE STANDARD DEVIATION ABOUT THE MEAN

SMALL VALUE OF
DISTINGUISHABILITY
MEASURE

194

AN EXAMPLE OF A "GOOD" FEATURE

LARGE VALUE OF
DISTINGUISHABILITY
MEASURE

196

AN EXAMPLE OF A BAD FEATURE

FIG. 26

CENTER-LINE OFFSET
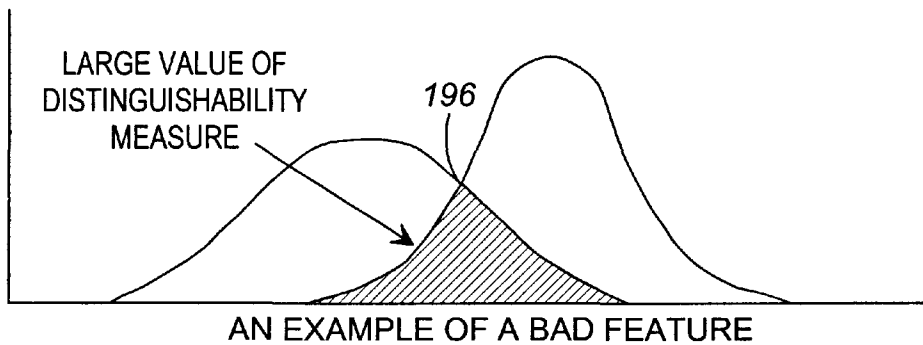
206

204

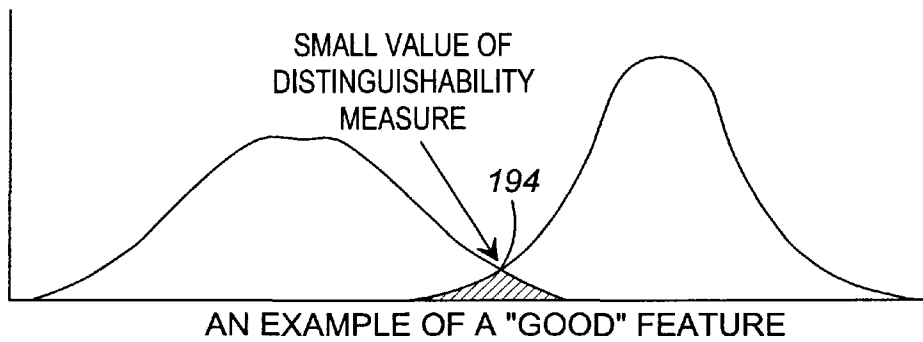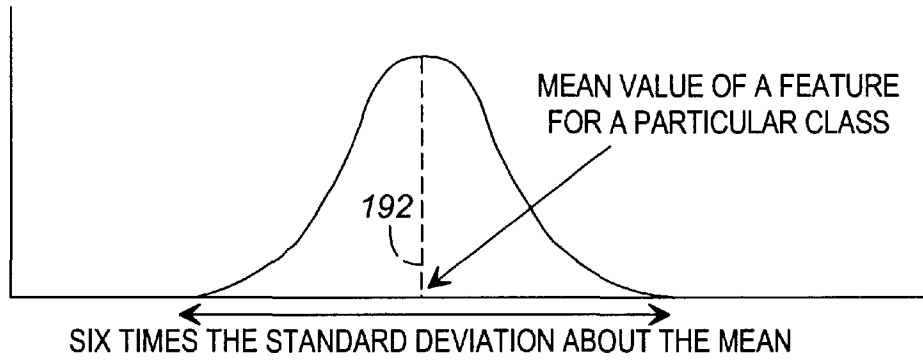SOLDER PADS

204

FIG. 27

202   202   IC LEADS   202

BOND VALIDATION OF SURFACE MOUNT DEVICES
GEORGIA INSTITUTE OF TECHNOLOGY - PROJECT RESEARCH LAB

BOND VALIDATION: MAIN MENU

A-) REINITIALIZE AD1000'S

C-) CREATE A NEW FILE

O-) OPEN EXISTING FILE

I-) INITIALIZE THE TABLE

R-) REVIEW FILE

T-) TEACH POSITIONS

N-) INFRARED ANALYSIS

V-) VISION ANALYSIS

M-) IMAGE CAPTURE

P-) PLOT DATA/IMAGES

D-) DISPLAY TIF FORMAT CAPTURED IMAGE

E-) EDIT AS TEXT FILE

Q-) QUIT

CHOOSE BY LETTER:

FILE: <NONE>

FIG. 28

FIG. 29

FIG. 30

FIG. 31
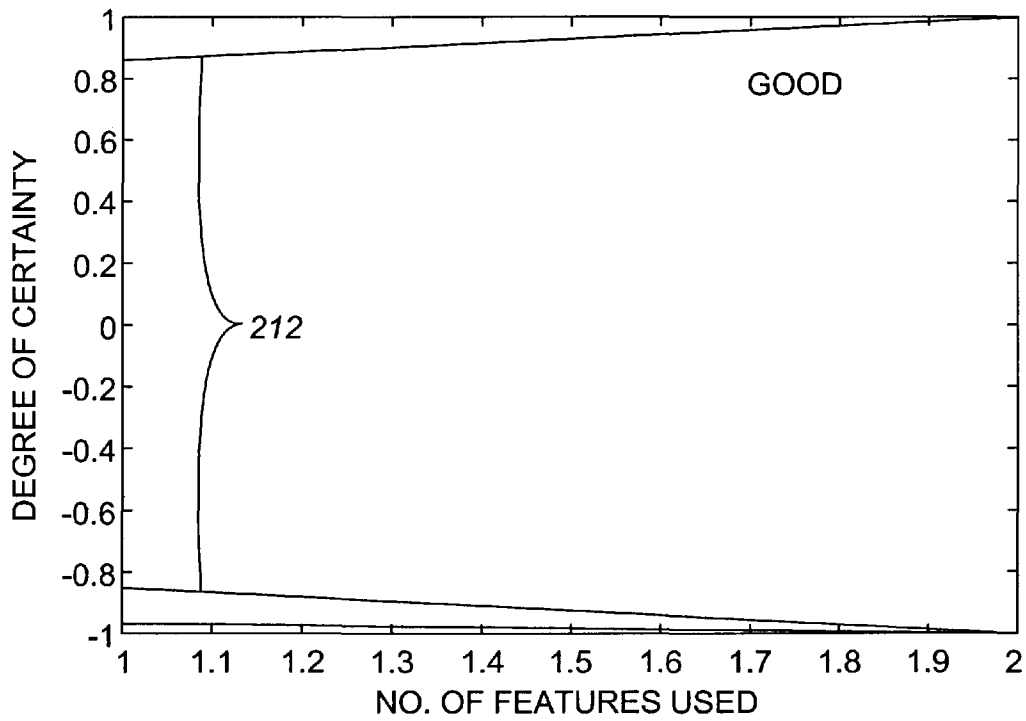
FIG. 32

FIG. 33

FIG. 34

FIG. 35

INSPECTION SYSTEM AND METHOD FOR BOND DETECTION AND VALIDATION OF SURFACE MOUNT DEVICES
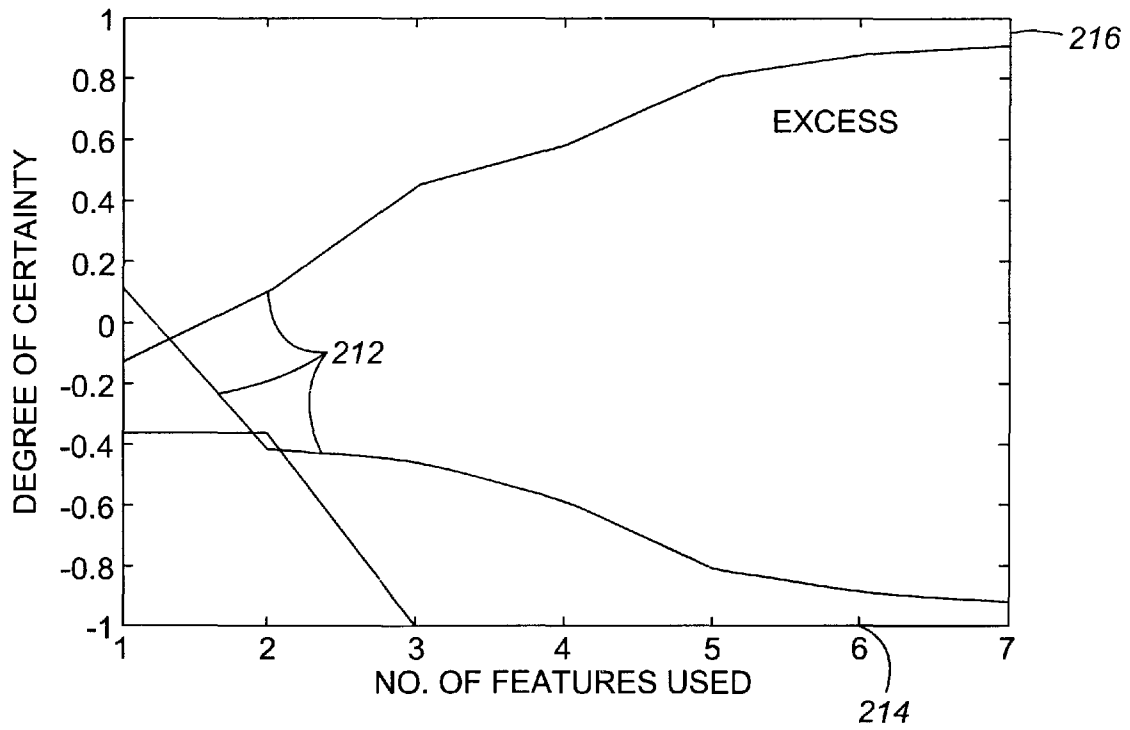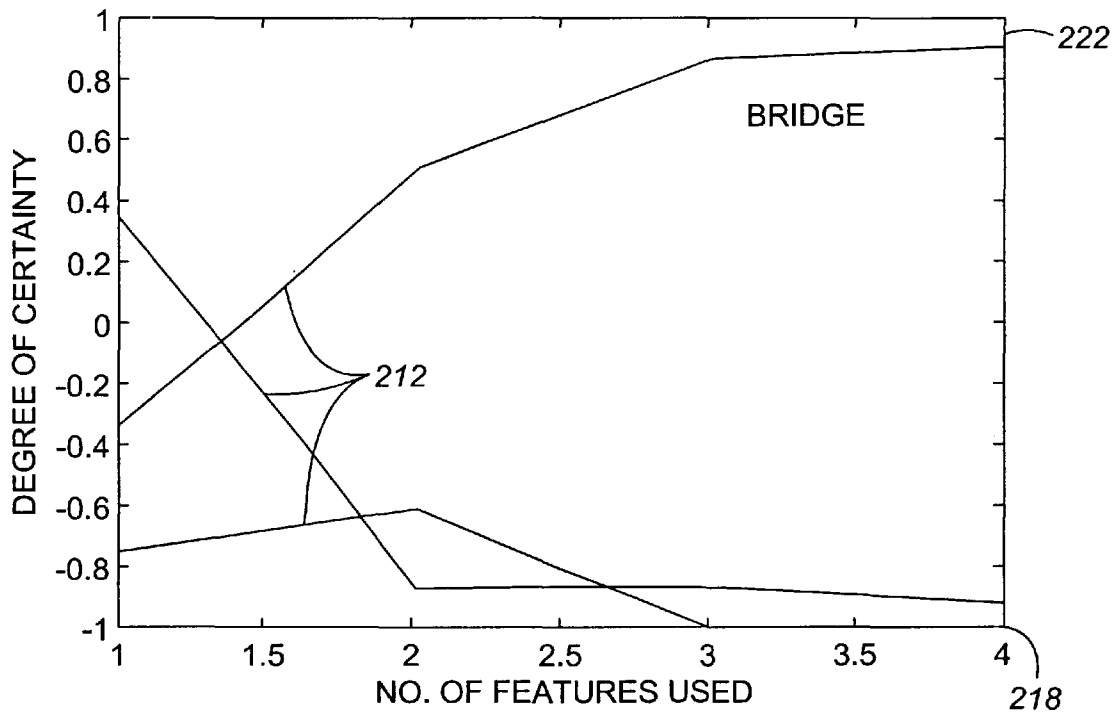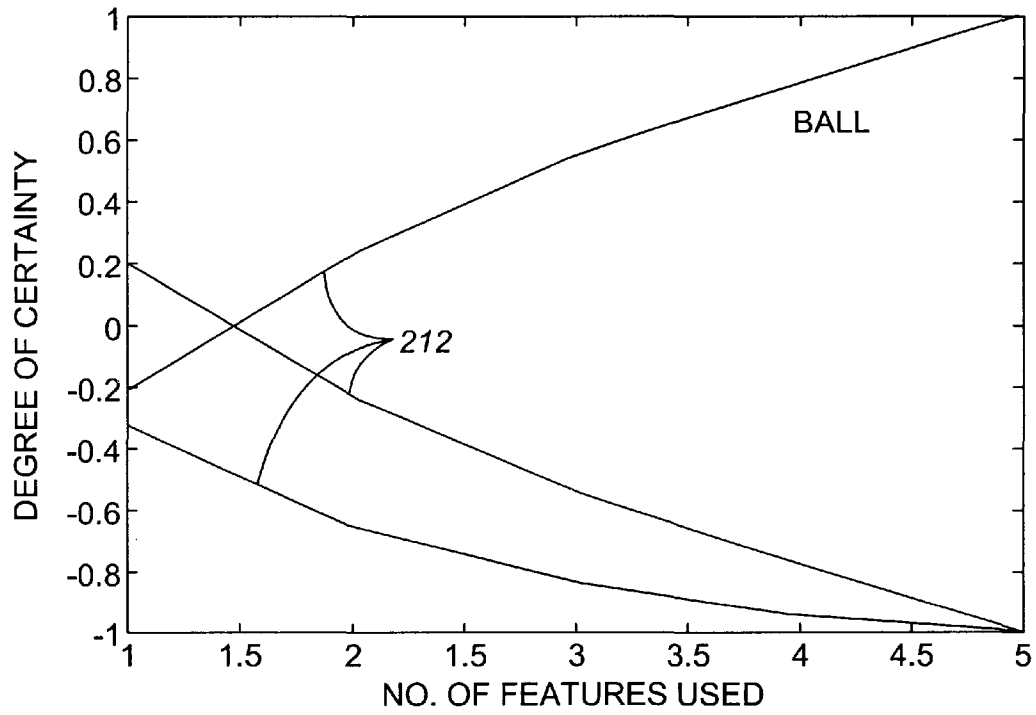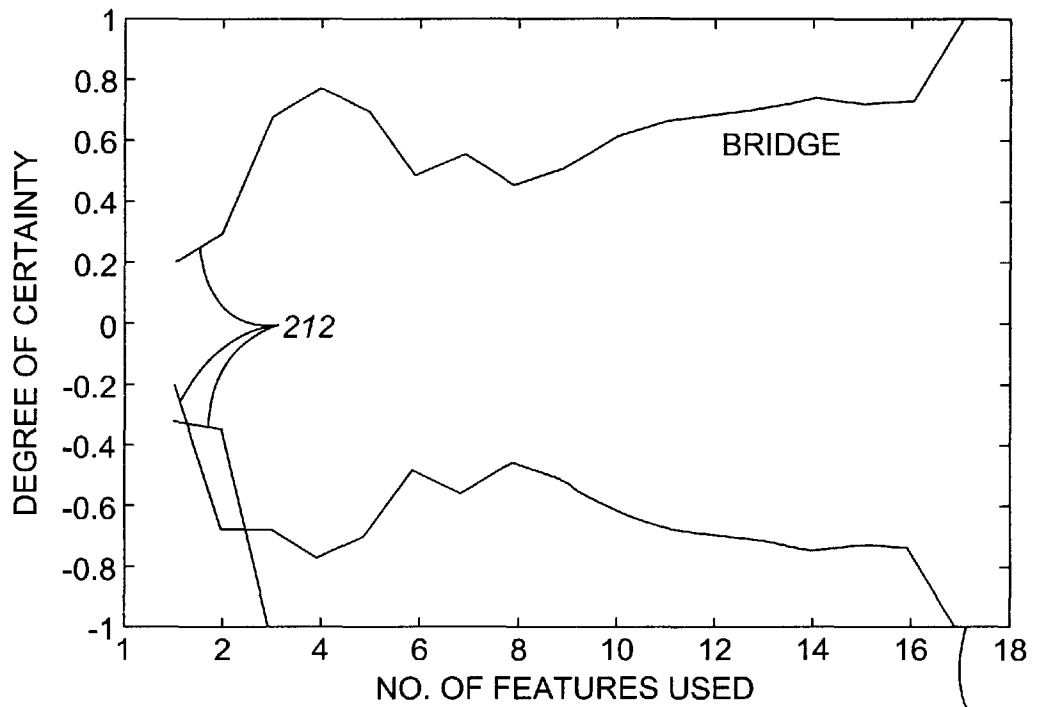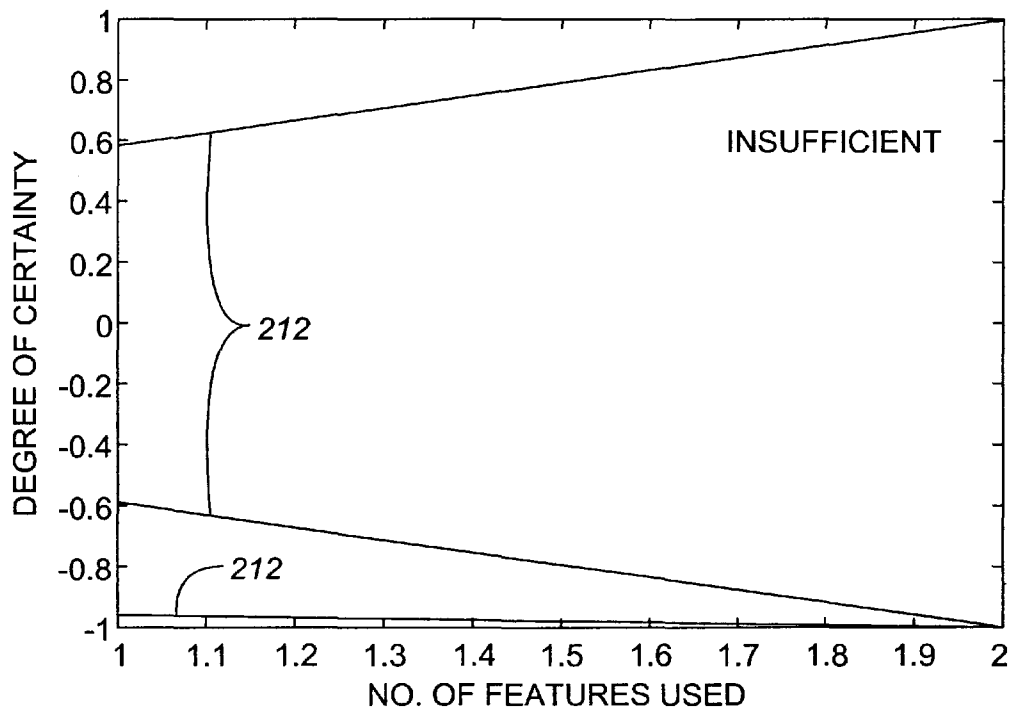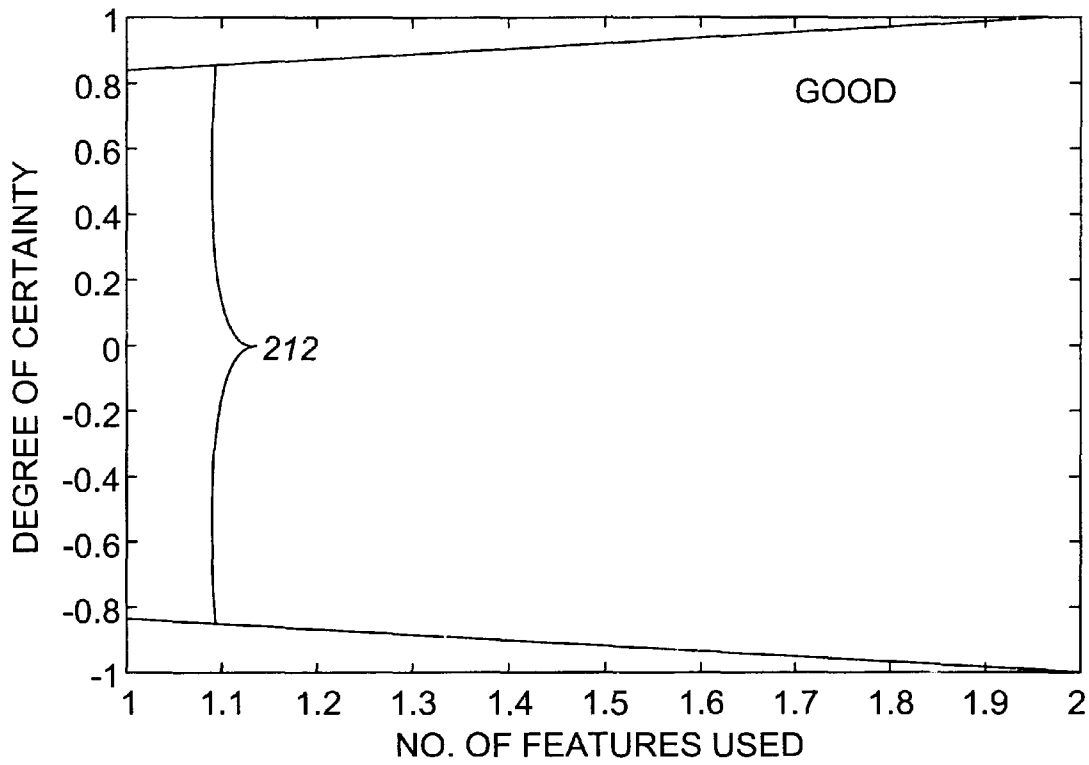
CROSS REFERENCE TO RELATED APPLICATION

This application claims benefit of the filing date of previously filed provisional application entitled INSPECTION SYSTEM AND METHOD FOR BOND DETECTION AND VALIDATION OF SURFACE MOUNT DEVICES, Ser. No. 60/023519, filed Aug. 7, 1996.

FIELD OF THE INVENTION

The present invention relates generally to quality control inspection systems and more particularly, to an inspection system and method for bond detection and validation of surface mount devices using vision and infrared sensors, combined with a technique for discriminating and detecting solder joint defects.

BACKGROUND OF THE INVENTION

It is indeed paradoxical that, on one hand, the quality of manufactured printed circuit boards (PCBs) has increased steadily over the past years while, on the other hand, the need for quality assurance has become more pronounced. As packaging technology marches on from through hole to surface mount to multichip modules, the complexity and sophistication of these processes introduce a larger aggregation of defect categories and impose stringent performance requirements. The critical role of electronic devices in diverse application areas such as missiles, aircraft, automotive manufacturing, computers and communications, etc. necessitates means for "proof-of-reliability" and metrics of performance. In the case of surface mount technology (SMT), finer pitch leads have increased the complexity of PCBs beyond the point of accurate and repeatable manual inspection. Many studies have been performed that show on a given day, an operator may inspect the same PCB and declare different defects. This lack of reliability and repeatability demands a more accurate approach using automated systems. The most widely used methods for automated inspection are based on vision, infrared (IR),and X-ray. Vision systems are relatively mature but are limited to surface level defects and cannot detect structural defects such as voids. P. J. Besl, et al., "Automated Visual Solder Inspection", IEEE Transactions on Pattern Analysis Machine Intelligence, vol. PAMI-11, pp.42–56, March 1985, D. W. Capson and S-K Eng, "A Tried Color Illumination Approach for Machine Inspection of Solder Joints", IEEE Transactions on Pattern Analysis Machine Intelligence, vol PAMI-10, pp.387–393, May 1988 and S. L. Bartlett, et al., "Automatic Solder Joint Inspection," IEEE Transactions on Pattern Analysis Machine Intelligence, vol. PAMI-10, pp.32–42, January 1988. Vanzetti used IR for inspection employing the radiance of the material to determine the mass of solder present. This method is not capable of reliably detecting surface level defects such as linear misalignment and angular misalignment. Riccardo Vanzetti and Alan C. Traub, "Combing Soldering with Inspection", IEEE Control Systems Magazine, pp.29–31, October 1988. The X-ray based inspection uses radiographic imaging techniques to obtain X-ray images of the solder joints for defect classification. M. Juha, "X-ray Machine Vision for Circuit Board Inspection," Proceedings of Vision 86 Conf. of SME, Detroit, Michigan, pp.3-41–3-55, June 1986. The X-ray based inspection is reliable in its scope of coverage, but it is

very costly and still cannot detect all the defects. The limitations of automated systems are caused by the scope of the individual sensors in classifying the known range of defects. Kenneth Reid, "Automated Soldering Inspection Technology Study," Proceedings of Technology Program of NEPCON West, Anaheim, California, vol. 3, pp.1288–1297, February 1993. The complementary nature of IR and vision sensors improves the reliability of the inspection scheme and broadens the scope of quality assurance strategies. The use of multiple sensors requires a system to fuse the information, process it for classification, and ultimately provide feedback to the process. For the system to have practical application, it should be cost effective, and operate in a timely fashion.

A low-cost, robust, flexible and accurate inspection system for detecting and identifying surface mount defects is needed. Inspection requirements vary from one industry sector to another just as the products to be inspected exhibit an enormous range of variability, however there is no universal definition of a good solder joint. In order to meet such diverse requirements, it was decided to design, develop and implement an inspection system that utilizes the synergism and complementarity of vision and IR sensing in a unified platform that may carry out an inspection task on the basis of either 100% testing or a sampled population. The inspection procedure is performed in two stages in order to reduce the inspection time and to have control over the production line delays. The first stage is called a GROSS inspection station that scans a PCB to determine global features to find probable defective areas of the PCB. The second stage is a FINE inspection station that uses intensive methods on questionable areas and generates local features for classification. Since the FINE inspection is performed off-line, it does not create a bottleneck in the production process. The complementary nature of the vision and IR sensors allows a broad range of classifications that would not be possible using only one sensor. This fusion combined with an on-line and off-line inspection procedure, offers a reliable and time efficient system for solder joint inspection.

SUMMARY OF THE INVENTION

A hybrid inspection system which includes vision and IR sensors. The vision sensors are gray scale charge coupled device (CCD) cameras which take 640×480, 256 gray scale 2-dimensional images of the solder joints. The visual inspection techniques include image processing and pattern recognition approaches for automatic inspection of visible defective joints. The IR side of the system uses a laser to heat the joint and observe the IR radiance curve as the joint heats and cools. The IR radiance curve is called a thermal signature of the joint. A two color IR sensor is used to record the thermal signature of a solder joint. The two color IR sensor is used to get emissivity independent thermal signatures by performing data level sensor fusion.

The GROSS inspection station is employed first on-line, to rapidly detect defects such as missing components, angular misalignment, linear misalignment, and solder mass related defects on a sample basis. A vision system checks for the component's presence and for placement related defects. After these defects have been screened, a statistical sampling scheme is used for IR screening to detect defect categories such as excess solder, insufficient solder, no solder and lifted leads. At this stage, the complete thermal signature of the solder joints is captured, but only the difference between starting and peak value, and the difference between peak and final value is analyzed to determine if it falls within normal range. If a potentially defective board is recognized, the candidate PCB is shipped to the FINE inspection station

where another vision system captures a higher resolution two-dimensional 256 gray level image of the probable defective areas and exhaustive defect search is performed at the lead level. For the IR inspection, the complete thermal signature, stored at the GROSS inspection station, is analyzed both in the heating and cooling cycles and the defect, if there is one, is declared and classified. The trade-off here is between speed of inspection and thoroughness. The statistical sampling scheme is used to cut down the time required to inspect each joint. The sampling rate can be adjusted to meet the constraints of the process. Sensor fusion techniques have been developed to combine vision and IR sensors' data at various levels of abstraction. A data level sensor fusion methodology for two IR sensors provides emissivity independent thermal signatures of the solder joints. At the FINE inspection station, active perception is employed to perform feature level sensor fusion.

Other features and advantages of the present invention will become apparent to one of skill in the art upon review of the following drawings and the detailed description of the preferred embodiments.

BRIEF DESCRIPTION OF THE DRAWINGS

The present invention, as defined in the claims, can be better understood with reference to the following drawings. The drawings are not necessarily to scale, emphasis instead being placed on clearly illustrating principles of the present invention.

FIG. 1 illustrates the proposed assembly line inspection system for surface mount devices.

FIG. 2 illustrates the block diagram of combined vision/IR inspection system.

FIG. 3 illustrates the hardware configuration of combined vision/IR inspection system.

FIG. 4 illustrates the block diagram of GROSS Inspection procedure.

FIG. 5 illustrates a PCB image with directional front illumination.

FIG. 6 illustrates histograms of the dark side for component present and absent cases.

FIG. 7 illustrates perceptron results for component presence test.

FIG. 8 illustrates a typical PCB image using diffuse front illumination

FIG. 9 illustrates a binary image of the leads of one side of an IC.

FIG. 10 illustrates the max scan at different stages of morphological filtering.

FIG. 11 shows an illustration of angular misalignment defect detection.

FIG. 12 illustrates the graphical representation of linguistic labels, ZERO, POSITIVE, NEGATIVE, VERY POSITIVE, and VERY NEGATIVE, as fuzzy sets.

FIG. 13 illustrates a typical thermal signature of a solder joint.

FIG. 14 illustrates spectral radiant emittance curves at different temperatures and.

FIG. 15 illustrates blackbody spectral radiant emittance at different temperatures, superimposed on InSb and MCT detectors' sensitivity.

FIG. 16 illustrates the Z signal.

FIG. 17 illustrates the Z signals of good and defective solder joints.

FIG. 18 illustrates the feature space for IR based GROSS inspection.

FIG. 19 illustrates the block diagram of FINE inspection procedure.

FIG. 20 illustrates good solder joints and typical solder joints defects.

FIG. 21 illustrates a sequence of nested subsets of $\ominus$.

FIG. 22 illustrates the flow chart of DOC calculation procedure.

FIG. 23 illustrates DOC trajectories for class A.

FIG. 24 illustrates the active perception procedure for defect classification.

FIG. 25 illustrates the mixture probability density function of a feature for two class case.

FIG. 26 illustrates the graphical representation of distinguishability measure.

FIG. 27 illustrates the centerline offset feature for a linearly misaligned IC.

FIG. 28 illustrates a menu screen of the vision/IR inspection system.

FIG. 29 illustrates DOC trajectories for an excess solder defect.

FIG. 30 illustrates DOC trajectories for a bridging defect.

FIG. 31 illustrates DOC trajectories for a solder ball defect.

FIG. 32 illustrates DOC trajectories for a good solder joint.

FIG. 33 illustrates DOC trajectories for a bridging defect.

FIG. 34 illustrates DOC trajectories for an insufficient solder defect.

FIG. 35 illustrates DOC trajectories for a good solder joint.

DETAILED DESCRIPTION OF THE PREFERRED EMBODIMENT

With reference now to the figures wherein like reference numerals designate corresponding parts throughout the several views, FIG. 1 is a view of the proposed assembly line inspection system 20 for surface mount devices and FIG. 2 is a block diagram of the combined vision/IR inspection process. The GROSS inspection station 21 is employed first on-line, to detect missing components, angular misalignment, linear misalignment, and solder mass related defects. A vision system 23 inspects for component presence and placement related defects. Once these defects have been screened, a statistical sampling scheme is used for IR screening to detect defect categories such as excess solder, insufficient solder, no solder and lifted leads. The laser 27 heats the solder joint under inspection while the IR detector 26 captures a complete thermal signature of the solder joint. At this time, only the difference between starting and peak value, and the difference between peak and final value is analyzed to determine if it falls within normal range. If a potentially defective board is recognized, the candidate PCB is shipped to the FINE inspection station 28 where another vision system 29 captures a higher resolution two-dimensional 256 gray level image of the probable defective areas and an exhaustive defect search is performed at the lead level. For IR analysis, the complete thermal signature, stored at the GROSS inspection station, is analyzed both in the heating and cooling cycles and the defect, if there is one, is declared and classified. The statistical sampling scheme is used to reduce the time required to inspect each solder joint. The sampling rate can be adjusted to meet the constraints of

the process. Sensor fusion techniques have been developed to combine vision and IR sensors' data at various levels of abstraction. A data level sensor fusion methodology for two IR sensors provides emissivity independent thermal signatures of the solder joints. At the FINE inspection station, active perception is employed to perform feature level sensor fusion.

FIG. 3 illustrates the principal components of the combined IR/Vision inspection system 10. The experimental setup for the IR inspection utilizes a Nd:YAG 1.06~\μm, 100 W, class IV laser 12 to heat the solder joints, and a two color EG\&G Reticon IR sensor 14 to sense the thermal radiation of the joints. The IR sensors used are Indium Antimonide (InSb) and Mercury-Cadmium-Telluride (MCT), which are sensitive in the 2–5 μm wavelength range and the 6–10 μm range, respectively. The sensor is cooled using liquid nitrogen. Two vision systems are used, one for the GROSS inspection station and one for the FINE inspection station. The GROSS inspection station vision system consists of a ⅔ inch CCD camera 16, a 24 mm telecentric lens, a 9 inch monochrome monitor, and a frame grabber capable of capturing 640×480, 256 gray level images. In general, the solder joint is brighter, and therefore has a higher overall gray scale value than the substrate. The substrate is commonly a shade of green. To assure high quality absorption of the incident light by the substrate, a red-pass filter is used in the illumination. To have uniform shadow free illumination, a circular fiber optics ring light is used. For oblique illumination, a fiber optics goose neck is employed. The FINE inspection station vision system consists of the same setup as that of the GROSS inspection station except for the lens. The lens of FINE inspection station is microscopic lens with variable magnification ratios from 0.7× to 4.5×. An X-Y positioning table 18 with 30 inch travel, is used for moving the PCB under test. The two vision systems, the IR system and X-Y positioning table are controlled by a 90 MHz Pentium based personal computer 22.

GROSS Inspection Software

This section details the software developed for the GROSS inspection station. The software has been developed for defect detection and identification, sensor fusion, and control of the overall system. The various preprocessing and recognition modules for the GROSS inspection have been implemented such that they communicate and transfer information sequentially to perform the comprehensive GROSS inspection. FIG. 4 illustrates the flow diagram 30 of the GROSS inspection procedure.

The GROSS inspection station has been designed as a conservative inspection procedure to insure no defective solder joints are declared as good. The defect detection performed at this stage uses vision data and IR thermal signatures in a complementary manner. Since IR can reliably detect the solder mass related defects, it is used to detect the solder mass related defects, such as bridging, excess solder, insufficient solder, cold joint, and lifted leads. The vision GROSS inspection station is used to detect missing components, and component placement related defects such as angular misalignment, and linear misalignment.

Vision Based GROSS Inspection

Referring now to FIG. 4, the vision data system consists of a two-dimensional 256 gray scale image of the PCB. A pattern recognition methodology is employed to detect different types of solder joint defects using these images. Both crisp and fuzzy classifiers have been investigated for defect detection at this stage. The first step in the inspection process of a PCB is to determine whether the components are present on the board 34. Once the component presence is

determined, its linear alignment 38 and angular alignment 42 is checked. To perform these tests, two images are captured at each programmed location. These locations are programmed during the off-line training phase. The first image is captured using a directional front illumination technique 32 for the components' presence test. The second image is captured using a diffused front illumination approach 36 for linear and angular misalignment tests.

Component's Presence Test

To detect the component presence and absence efficiently and reliably, features were found that were able to discriminate between the presence and absence of a component. Since the components are three-dimensional objects, while the solder pads underneath are two-dimensional, techniques were considered to exploit this disparity and generate the desired features. Using a directional front illumination technique, the detection of component's presence or absence can be performed effectively and in a timely fashion. The PCB is illuminated by projecting a goose neck halogen light source at approximately 30° from the PCB plane. If the component is present, a shadow is cast. FIG. 5 illustrates the shadow cast by a present component 52 and the lack of a shadow on the missing component 54.

The side of the component toward the light source is called the bright side, and the side with the shadow is called the dark side.

Sub-images are extracted by using rectangular windows on all the sides of a component. The windows are defined such that they contain areas specified for the leads of that component. The normalized histogram of each sub-image is calculated and appropriate features are extracted for classification. Referring to FIG. 6, the normalized histogram 60 of the dark side of a component present case 62 and a component absent case 64 are shown.

The features extracted for component presence test are the expected value and the standard deviation of the normalized histogram. Since the feature space is linearly separable, a perceptron classifier 70 is selected for classification. The training data set for the perceptron consisted of 28 exemplars while the evaluation set consisted of six data values. Referring to FIG. 7, the training data 72, validation data 74 and the class boundary 76 is shown.

Linear Misalignment Test

The shadow free images of a PCB are captured using flat a illumination source. A red-pass filter is added to a light source to enhance the contrast of the green substrate and solder joints. FIG. 8 illustrates a typical surface mount component image.

Programmed rectangular windows are used to get sub-images of the solder joints 71 of the components 73. From each sub-image a one-dimensional vector is obtained such that the information about component leads and their placement location on the solder pads is preserved. This vector is called a max scan. The peaks of the max scan represent solder joints and solder pads while valleys represent the substrate. To obtain a max scan from a sub-image, first the sub-image is segmented using a threshold. Since the histogram is bimodal, threshold selection is easy. FIG. 9 illustrates a binary image of one side of an integrated circuit's leads.

Consider an image I of size M×N, represented as pix(i,j), i=1, . . . , M, j=1, . . . , N. pix(ij) is the pixel value at location (i,j) in I. Let S={$S_1,S_2, . . . ,S_j, . . . ,S_N$} be the max scan of I in the horizontal direction. The jth entry of S is calculated as

$$s_j = \max_{k=1}^{M-Q+1} (a_{jk}),\tag{1}$$

where α_{jk} is the average of the kth set of Q number of pixels in the jth column of I. The α_{jk} is calculated as

$$a_{jk} = \frac{1}{Q}\sum_{i=0}^{Q-1} pix(k+i.j).\tag{2}$$

For a horizontal max scan, Equation 2 acts as a low pass filter in the vertical direction of the image I. By changing the value of Q, the filter cut-off frequency can be changed.

A max scan may have noisy peaks and valleys. To filter out such peaks and valleys, a morphological filter is applied to the max scan. The mathematical morphology is a tool for extracting two-dimensional image components that are useful in the description of the region shape such as boundaries, skeleton, and convex hull. It can also be used for pre- and post-processing, such as morphological filtering, thinning, and pruning. R. Gonzalez and R. Woods, Digital Image Processing, Addison-Wesley Publishing Company, Reading, Mass., 1992. The mathematical morphology can be applied to one-dimensional data also. Let S_M be the output of the morphological filter, which is represented as,

$$S_M=(((S \ominus B) \oplus B) \oplus B) \ominus B,\tag{3}$$

where B is the structuring element, (symbol bigodot0 is the erosion operation, and $\oplus$ is the dilation operation. For set X and Y in Z^1 one-dimensional space, the erosion of X by Y is defined as

$$X \ominus Y = \{x|(Y)_x \subseteq X\},\tag{4}$$

which means that the erosion of X by Y is the set of all points x such that Y translated by x is contained in X. Mathematically, the translation of Y by x is defined as,

$$(Y)_x = \{c|c=y+x, \text{ for } y \in Y\}.\tag{5}$$

The dilation of X by Y is defined as

$$X \oplus Y = \{x|(\hat{Y})_x \cap X \neq \phi\},\tag{6}$$

which means that the dilation of X by Y is the set of all x translations of $\hat{Y}$, such that $\hat{Y}$, and X overlap by at least one nonzero element, where $\hat{Y}$ represents the reflection of Y, defined as

$$\hat{Y}=\{c|c=-y, \text{ for } y \in Y\}.\tag{7}$$

Referring now to FIG. **10**, the noisy peaks **82** and valleys **84** in the original max scan **86** are removed by the morphological filtering. After the morphological filtering, connectivity analysis is performed to determine the length of each bright and dark region encountered in the max scan **88**. The number of peaks encountered gives information about the components' leads detected. The length of the bright region corresponds to the width of the solder joint and the length of a dark region corresponds to the distance between two adjacent solder joints. A fuzzy relation and linguistic variable based classifier, explained in the next section, has been developed to detect linear misalignment defects. A fuzzy classifier has been used to accommodate the uncertainty associated with the misalignment defect definition.

Angular Misalignment Test

Using the same segmented sub-image as used for the linear misalignment test, the outside corners of the first and last solder pad in the sub-image are determined using a search algorithm. Also the outside corner of the component's first and last lead on that side is determined. Let solder pads' corners be (X_{p1},Y_{p1}) and (X_{p2},Y_{p2}). A line L_1 passing through these points has the slope, m_{pad}, given as

$$m_{pad} = \frac{y_{p2} - y_{p1}}{x_{p2} - x_{p1}}.\tag{8}$$

Seymour Lipschutz, Theory and Problems of Linear Algebra 2nd Edition, McGraw-Hill, Inc. 1991, ch.1, pp.1–38.

Similarly, the slope, M_{lead}, of the line passing through the outside corners of the component leads is determined. The difference of two slopes gives an error angle, calculated as follows:

$$\theta_{error}=|\tan^{-1}(m_{pad})-\tan^{-1}(m_{lead})|\tag{9}$$

where $|\cdot|$ is an absolute operation. The θ_{error} is then compared with a predetermined threshold for the declaration of an angular misalignment defect. Referring to FIG. **11**, an angular misalignment defect having A **92** and B **94** as the outside corners of solder pads and C **96** and D **98** as the outside corners of the component's leads.

Defect Identification using Fuzzy Relations and Linguistic Variables

To identify the defective solder joints at the GROSS inspection stage, a fuzzy classification approach using fuzzy relations and linguistic variables is used. This classification scheme works on linguistic labels rather than numerical quantities and underlines a generality of the construction performed. Often pattern description is provided in a linguistic manner rather than precise numerical quantities. For example, a statement formulated by a human being with respect to recognition of a class ω would be, "If the object size is LARGE and its speed is FAST, then it belongs to class ω." The size and speed are linguistic variables taking values expressed as linguistic labels such as LARGE, SMALL, FAST, SLOW, etc. The linguistic labels can be modeled as fuzzy sets on an appropriate universe of discourse.

Let X be the object to be classified having features that take linguistic values such as zero, positive, negative, etc. If there are N such features, then there is a fuzzy relation on the universe $Z=U_1 \times U_2 \times \ldots \times U_n \times \ldots U_N$ where U_n is the universe of discourse of the nth feature. Sankar K. Pal and D. Dutta Majumder, Fuzzy Mathematical Approach to pattern Recognition, John Wiley & Sons (Halsted), N.Y., 1986, ch. 3, pp 70–73. For fuzzy sets A, B on universe U, V, respectively, the membership of fuzzy relation A×B on universe U×V is defined as

$$\mu_{A \times B}(u,v)=\min\{\mu_A(u), \mu_B(v)\}, \forall u \in U, \forall v \in V\tag{10}$$

Lofti A. Zadeh, "Outline of a New Approach to the Analysis of Complex Systems and Decision processes", IEEE Transactions on Systems Man., Cybern., vol. SMC-3, no.1, pp.28–44, 1973.

where $\mu_A(u)$ is the membership of u in A and $\mu_B(v)$ is membership of u in B. Let the training set consist of L patterns partitioned into c classes, ω_k, for k=1, . . . , c. Let Ω_j, j=1, . . . ,L be a vector of size 1×c, representing the class membership of the jth pattern. The training patterns are expressed as fuzzy relations v_j, j=1, . . . ,L. By taking the Cartesian product of $\_j$ and Ω_j, j=1, . . . ,L, fuzzy relations are formed on the universe Z×[0,1]. The interval [0, 1]

represents the universe of discourse of Ω. The relation, R, for the fuzzy classifier is obtained by,

$$\mathcal{R} = \bigvee_{j=1}^{L} (\Upsilon_j \times \Omega_j) \tag{11}$$

where $\vee$ is the symbol for the maximum operator. The quantity $\gamma_j \times \Omega_j$ is obtained using (10). Given an unknown pattern X with feature values, $\Phi_1(X)$, $\Phi_2(X)$, . . . , $\Phi_N(X)$, its corresponding$_{13}$ is obtained and then its class membership_is calculated as,

$$\Phi = \gamma o R \tag{12}$$

where o is the composition rule of inference. Lofti A. Zadeh, "Outline of a New Approach to the Analysis of Complex Systems and Decision processes", IEEE Transactions on Systems Man., Cybern., vol. SMC-3, no.1, pp.28–44, 1973.

Referring now to FIG. **12**, let us consider the extracted features which are, solder joint width and the distance between two adjacent solder joints. Let the features be represented as a vector $X=\{x_1, x_2\}$ where x_1 is solder joint width and x_2 is the distance between the adjacent solder joints and the templates be represented as $T_k=\{t_{k1}, t_{k2}\}$, k=1, . . . , p, where p is the surface mount components' type to be inspected. The templates are generated during the off-line training of the system. For the jth type surface mount component under inspection, an error vector $E=\{e_1, e_2\}$ is calculated where $e_1=x_1-t_{j1}$ and $e_{2=x2}-t_{j2}$, which are the linguistic variables taking values expressed as linguistic labels ZERO 91, POSITIVE 93, NEGATIVE 97, VERY POSITIVE 99 and VERY NEGATIVE 101. FIG. **12** illustrates these linguistic labels represented as fuzzy sets.

The fuzzy relations, γ, are constructed using the a priori information about specific good and defective solder joints. During the off-line training phase, the system generates the fuzzy relation R for the classifier. The training is completed in only one pass through the training data set.

IR Based GROSS Inspection

The purpose of the IR sensors in the GROSS inspection station is to detect subsurface and solder mass related defects. These defects include voids, insufficient, no solder, excess solder, solder ball, and bridging. These defects exhibit the gross characteristics of a significant variance in the amount of solder present on the component, since the IR signal is a function of the radiance of the component. I. Dar, K. Newman and G. Vachtsevanos, "Bond Validation of Surface Mount Components Using a Combined IR/Vision System", Applied Machine Vision 94 Conference of SME, Minneapolis, Minnesota, vol. 2, session 7, June 1994. The solder mass related defects can be divided into two general categories: excess solder mass, and insufficient solder mass. The excess solder mass category includes defects such as excess solder, solder ball, and bridging whereas the insufficient solder mass category includes defects such as voids, insufficient, and no solder. The IR based GROSS inspection identifies whether the solder joint under test is good or it belongs to one of two defect categories. Before explaining the details of IR based GROSS inspection algorithms, the emissivity dependence of a thermal signature, a limitation of IR based solder joint inspection, is discussed. A data-level sensor fusion methodology has been developed to obtain emissivity independent thermal signatures of solder joints.

Emissivity Dependent Thermal Signature

Referring to FIG. **13**, the IR technology utilizes IR thermal signatures of solder joints for inspection. These signatures are produced when a laser heats an individual

solder joint and an IR sensor records its thermal radiation curve **103**, called IR thermal signature or simply thermal signature. The thermal signature of a solder joint is a time series.

A problem associated with thermal signature analysis is that the sensor measurements are dependent on the emissivity of the solder joint. The IR radiant emittance, W, of a target is given as

$$W = \in \sigma T^4, \tag{13}$$

J. M. Lloyd, Thermal Imaging Systems, Plenum Press, New York, 1975.
where $\in$ is the emissivity, T is temperature in degrees Kelvin, and σ is the Stefan-Boltzmann constant which is equal to 1.38054×10^{-23}. For an ideal blackbody, $\in$ is equal to 1.0. The objects with radiation curves similar to those of a blackbody, but lower, are called graybodies. The ratio between the actual radiant emittance of an object and that of the blackbody value is the emissivity. Mathematically,

$$\epsilon = \frac{W_{actual}}{W_{ideal}}. \tag{14}$$

The emissivity of unoxidized solder is between that of unoxidized tin (0.043) and unoxidized lead (0.05). CRC handbook of Chemistry & Physics, CRC Press Inc., Boca Raton, 49th edition, pp. E227. The emissivity of a solder joint can vary substantially because of differences in surface finish (i.e., a rough finish has higher emissivity because of greater absorption), the presence of pinholes, vents or blowholes, or surface contamination. The surface contamination may be present as genuine contamination or as normally occurring flux residues in a no-clean process. Varying emissivity changes the thermal signature of a joint in two ways. First, it increases the temperature rise of the joint because a higher emissivity surface absorbs more impinging radiation. Second, at a given temperature, the radiance is increased in direct proportion to the emissivity increase. These variations of emissivity add a random noise to the sensor measurement.

Fusion of IR Detectors

A sensor-fusion approach at data level has been developed to obtain emissivity-independent thermal signatures using two IR detectors sensitive in different radiation wavelengths. Planck's equation for the spectral distribution of a blackbody radiation provides a model of the radiance of a blackbody as a function of temperature and wavelength. It is given as

$$W_\lambda = \frac{C_1}{\lambda^5 \left(\exp\left(\frac{C_2}{\lambda T}\right) - 1 \right)}, \tag{15}$$

J. M. Lloyd, Thermal Imaging Systems, Plenum Press, New York, 1975. where λ is the wavelength in μm, T is the temperature in degrees Kelvin, C_1 and C_2 are constants with values equal to 3.7415×10^4 and 1.4388×10^4, respectively. Referring to FIG. **14**, three curves related to Equation 15 are depicted. The solid lines **102** show the spectral radiant emittance curves for a blackbody, while the dotted line **104** illustrates a spectral radiant emittance curve of a graybody with emissivity equal to 0.85.

The total radiance of a graybody at a given temperature is the area under its spectral radiant emittance at that temperature, i.e., the graybody spectral radiant emittance

summed over all wavelengths at a given temperature. Mathematically,

$$\mathcal{R} = \int_0^\infty \frac{\epsilon C_1}{\lambda^5 \left(\exp\left(\frac{C_2}{\lambda T}\right) - 1 \right)} d\lambda. \tag{16}$$

An IR detector functions by integrating the intensity of all wavelengths to which it is sensitive. For example, an Indium Antimonide (InSb) based IR detector is sensitive in the 2–5 μm range. Equation 16 for an InSb detector, can be written as

$$\mathcal{R} = \underbrace{\int_1^5 \frac{\epsilon C_1}{\lambda^5 \left(\exp\left(\frac{C_2}{\lambda T}\right) - 1 \right)} d\lambda}_{v} + \mathcal{N}, \tag{17}$$

where N represents radiance outside the sensitive band of the detector, v is the output voltage of the sensor that represents the IR energy in the detector's sensitive band. Due consideration should be given to the information being lost because of the IR detector bandwidth limitations. The MCT detector is sensitive in the 6–12 μm range. Referring now to FIG. 15, the blackbody spectral radiant emittance curves for 25° C. 112, 50° C. 114, and 75° C. 116 are superimposed on the sensitivity curves of an InSb detector 118 and a Mercury-Cadmium-Telluride (MCT) detector 119. FIG. 15 illustrates that a large portion of the radiance curves lies within the two detectors' sensitive range. Since solder joints are heated to 75° C. or less for inspection purposes, it is more appropriate to use both the IR detectors to measure the thermal signature of solder joints. For the two IR detector cases, Equation 16 becomes

$$\mathcal{R} = \underbrace{\int_1^5 \frac{\epsilon C_1}{\lambda^5 \left(\exp\left(\frac{C_2}{\lambda T}\right) - 1 \right)} d\lambda}_{v_1} + \underbrace{\int_6^{12} \frac{\epsilon C_1}{\lambda^5 \left(\exp\left(\frac{C_2}{\lambda T}\right) - 1 \right)} d\lambda}_{v_2} + \mathcal{N}, \tag{18}$$

where v_1 represents the output voltage of InSb detector and v_2 represents the output voltage of MCT detector. Notice that in Equation 18 $\in$ is a constant with respect to the integral. The IR detectors' output is fused by taking the ratio of the detectors' output. Let Z be the ratio of the MCT detector's output and the InSb detector's output. Mathematically,

$$Z = \frac{\epsilon \int_6^{12} \frac{C_1}{\lambda^5 \left(\exp\left(\frac{C_2}{\lambda T}\right) - 1 \right)} d\lambda}{\epsilon \int_1^5 \frac{C_1}{\lambda^5 \left(\exp\left(\frac{C_2}{\lambda T}\right) - 1 \right)} d\lambda}. \tag{19}$$

In Equation 19, $\in$ cancels out, therefore Z is independent of the emissivity. Equation 19 can be written in terms of the detectors' voltage as

$$Z = \frac{v_2}{v_1}. \tag{20}$$

FIG. 16 illustrates the Z signal 111 obtained by fusing the outputs of the MCT and InSb IR detectors.

GROSS Inspection using Thermal Signatures

To identify solder joint defects using thermal signature, features are determined that maximize the variation between the good solder joint signature and the defective solder joint signature. In the insufficient solder mass category, there is a lack of solder; therefore, for the same laser heating time, the signature will be elevated because of an increase in IR radiation. For the excess solder mass category, there is an excess of solder, thereby decreasing the amount of the IR radiated from the joint and lowering the thermal signature. FIG. 17 illustrates the Z signals of solder joints of an integrated circuit.

The number of joints to be tested is determined prior to inspection by a random sampling scheme. This is a function of the perceptance of inspection to be performed. The amount of time required for the inspection of one joint is approximately 500 milliseconds. This takes into consideration the amount of time required to position the joint using X-Y table, fire the laser, collect the data, and process the information. The majority of the time is devoted to the collection of the signature which takes on average 400 milliseconds. Inspection of a largely populated board would be time consuming if 100% inspection was desired. This is the reason for the sampling methodology for on-line applications.

The two most noticeable and easy to obtain features in the Z signals are the differences between the starting point 113 and the maximum point 117, and the maximum point 117 and the end point 119. These features can be determined rapidly from the data. Referring to FIG. 18, the feature space 122 and the decision boundaries 124 for the GROSS inspection are shown. Since the feature space is linearly separable, a perceptron classifier has been designed to perform the classification.

FINE Inspection Software

The potentially defective solder joints, identified by the GROSS inspection, are analyzed more closely in order to confirm the joints' defects and classify them into defect categories. This classification is performed using information provided by the two-dimensional gray level images of the solder joints and their thermal signatures. The software developed for the FINE inspection station performs sensor fusion at feature level using an active perception approach. The active perception methodology developed for the FINE inspection not only fuses the complementary information obtained from the IR sensors and vision sensors but also minimizes the processing time by controlling the information gathering process. The premise used for this control is to acquire only that much information which is required to perform the task at hand. The active perception approach is generic in the sense that it can be applied to a multi sensor environment as well as to the features extracted from a single sensor.

FIG. 19 illustrates the block diagram of the FINE inspection procedure. The data acquisition module 132 consists of a vision sensor 134 and a two color IR sensor 136. The vision sensor provides high resolution two-dimensional images of the solder joints while the two color IR sensor generates thermal signatures of the joints. FIG. 20 illustrates an image of good solder joints and typical images of some of the solder joint defect categories.

13

The IR sensor data is fuised at the data level to obtain a Z signal, as explained in the previous section titled IR Based GROSS Inspection. A preprocessing module **138** includes an image processing means **137** for converting the images captured by the vision system, and a thermal processing means **139** for converting the thermal signatures recorded by the infrared sensors into a form from which characteristic features of different defect classes can be easily extracted. The pre-processing involves operations such as frequency domain filtering, spatial filtering and enhancement by noise removal. Since the FINE inspection is performed only if GROSS inspection detects a potential linear misalignment defect, excess solder mass defect, and/or insufficient solder mass defect, the FINE inspection procedure is broken down into three modules. These modules are linear misalignment test **142**, insufficient solder mass test **144**, and excess solder mass test **146**. The linear misalignment test **142** confirms whether the potentially defective joints are linearly mis-aligned. The insufficient solder mass test **144** classifies a potential defective joint into good, void, insufficient solder, or no solder categories. The excess solder mass test **146** classifies a potential defective joint into good, bridging, excess solder, or solder ball categories. The excess solder mass test **146** and the insufficient solder mass test **144** modules use the active perception methodology to perform feature-level sensor fusion for defect classification. Before presenting the details of each of these modules, the active perception for feature-level sensor fusion is explained.

Active Perception

Active perception can be defined as the problem of controlling one or more sensors during data acquisition to maximize the performance of the information-gathering process. Human perception is primarily governed by this concept. If we analyze the human perception process, it appears that perception involves adaptiveness and intelli-gence to reason and make decisions as quickly as possible. These attributes are desirable for machine perception as well, which usually involves processing a large number of data sets originating from one or more sensors.

The objective of active perception is to achieve reliable recognition in a minimum amount of time. The conventional machine perception or pattern recognition approach involves a sequence of steps, namely, data acquisition, feature extraction/selection, and classification. The feature extraction process converts the objects into an N-dimensional feature space, such that one class of objects is clustered together and can be distinguished from other classes. However, in general, not all objects of a class need N features to form a compact cluster. It is only the objects that are in the overlapping region of two or more classes that govern the number of features required to perform classifi-cation. If there is a way to judge the classifier result at each feature, then one could optimize the perception procedure by using that much information, which is sufficient for the task at hand. An index has been derived using the Dempster Shafer theory and fuzzy logic, which represents the faith or confidence committed to a classification result. This index is called degree of certainty (DOC).

Degree of Certainty

For a frame of discernment Θ and a proposition $A \subset \Theta$, the degree of certainty associated with A, DOC(A), is defined as

$$DOC(A) = m(A) - Bel(\bar{A}), \tag{21}$$

where m ($\cdot$) represents the mass function, Bel ($\cdot$) represents the belief function over Θ and $\bar{A}$ represents the complement of A.

14

The belief function over Θ is defined by Bel: $2^\Theta \rightarrow [0,1]$ and derived from the mass function m by

$$Bel(A) = \sum_{B \subseteq A} m(B) \quad \forall A \subseteq \Theta. \tag{22}$$

G. Shafer, A Mathematical Theory of Evidence, Princeton University Press, New Jersey, 1976.

The value of DOC indicates a relative amount of belief or confidence in the frame of discernment. The properties of DOC with appropriate explanations are given below.

DOC has a value in $[-1,1]$.

DOC(A)=1 indicates that the evidence supports A exclu-sively because m(A)=1 is always satisfied.

DOC(A)=0 is satisfied when m(A)=m(A), which implies that the amount of belief on A is equal to that of belief on the rest of Θ.

DOC(A)=−1 indicates that Pl(A)=1-Bel(A)=0, which implies that evidence does not support A at all.

From equation 21 it is clear that in order to calculate DOC associated with any one or more atomic propositions, the mass function needs to be determined first. Once the mass function for all the subsets of 2^Θ has been calculated, the belief function can be estimated for any subset of Θ by using Equation 22. Finally, the DOC for any subset of 2^Θ can be calculated using Equation 21.

Calculation of Mass Function

In this section, a systematic approach is derived using fuzzy logic and possibility measure to calculate mass func-tion on a frame of discernment. A family of subsets of a universal set is nested if these subsets can be ordered in such a way that each is contained within the next. Consider a body of evidence whose focal elements are nested. For such a body of evidence, the associated belief and plausibility measures are called consonant. G. J. Klir and T. A. Folger, Fuzzy Sets, Uncertainty, and Information, Prentice-Hall Inc., Englewood Cliffs, N.J., 1991. Consonant belief and plausibility measures are usually referred to as necessity measure and possibility measure, respectively. Let F={$x_1,x_2, \ldots,x_n$} be a body of evidence with n nested focal elements such that F={$A_i|A_1 \subset A_2 \ldots \subset A_n$}, where $A_i \in 2^F$. If π and η denote a possibility measure and a necessity measure on 2^F, respectively, then

$$\eta(A \cap B) = \min [\eta(A), \eta(B)] \forall A,B \in 2^F \tag{23}$$

and

$$\pi(A \cup B) = \max [\pi(A), \pi(B)] \forall A,B Å 2^F. \tag{24}$$

Every possibility measure π defined on 2^F can be uniquely determined by a possibility distribution function pd: F→[0, 1], as

$$\pi(A) = \max_{x \in A} pd(x) \quad \forall A \in 2^F. \tag{25}$$

G. J. Klir and T. A. Folger, Fuzzy Sets, Uncertainty, and Information, Prentice-Hall Inc., Englewood Cliffs, N.J., 1991.

Let a possibility distribution function pd be defined on a frame of discernment Θ={$x_1,x_2, \ldots,x_n$} with nested focal elements. A possibility distribution associated with pd is given as

$$pd = (\rho_1, \rho_2, \ldots, \rho_n), \tag{26}$$

where $\rho_i = pd(x_i)$ for all $x_i \in \Theta$. Assume that a possibility measure π is defined on 2^Θ in terms of its mass function m.

FIG. **21** illustrates a complete sequence of nested subsets of Θ **152** with associated mass function **154** and possibility distribution function **156**.

From the definition of possibility measure as consonant plausibility measure and using Equation 24 and Equation 25 it follows that

$$\rho_i = pd(x_i) = \pi(\{x_i\}) = Pl(\{x_i\})$$

for all $x \in \Theta$. The relationship between possibility measure and mass function is given as

$$Pl(A) = \sum_{A \cap B \neq \varnothing} m(B) \quad \forall\, A \subseteq \Theta, \tag{27}$$

G. Shafer, A Mathematical Theory of Evidence, Princeton University Press, New Jersey 1976.
where $\varnothing$ is the null set. Thus, it can be obtained from Equation 27

$$\rho_i = Pl(\{x_i\}) = \sum_{k=i}^{n} m(A_k) \tag{28}$$

since $x_i \in A_j \forall j \leq i$, a condition satisfied because of nested focal elements of Θ. Equation 28 can be written as a set of equations for $i = \{1, 2, \ldots, n\}$. These equations are

$$\rho_1 = m(A_1) + m(A_2) + \ldots + m(A_i) + \ldots + m(A_n)$$

$$\rho_2 = \quad\quad\quad m(A_2) + \ldots + m(A_i) + \ldots + m(A_n)$$

$$\vdots \quad\quad\quad\quad\quad\quad\quad\quad \vdots$$

$$\rho_i = \quad\quad\quad\quad\quad\quad m(A_i) + \ldots + m(A_n)$$

$$\vdots \quad\quad\quad\quad\quad\quad\quad\quad \vdots$$

$$\rho_n = \quad\quad\quad\quad\quad\quad\quad\quad\quad m(A_n).$$

Solving these equations for A_i, $i = \{1, 2, \ldots, n\}$, the relation between possibility measure and mass function is obtained as

$$m(A_i) = \pi(\{x_i\}) - \pi(\{x_{i+1}\}) \quad \forall \text{integer } i, \tag{29}$$

where $\pi(\{x_{n+1}\}) = 0$.

Zadeh founded the fuzzy set theory in which a fuzzy set is viewed as a basis for possibility theory. L. Zadeh, "Fuzzy sets as a basis for a theory of possibility", Fuzzy Sets and Systems, vol. 1, pp.3–28, 1978. Let Z be a fuzzy set of a universe of discourse U, which is characterized by the membership function μ_z with the grade of membership, μ_z (u)$\forall u \in U$. Let X be a variable taking values in U, and let Z act as a fuzzy restriction, R(X), associated with X. Then, the proposition "X is Z," which can be written as R(X)=Z, associates a possibility distribution, π_x with X, which is postulated to be equal to R(X), i.e., π_x=R(X). The possibility distribution function, pd_x, associated with π_x is defined to be equal to the membership function of Z. Thus, pd_x (u), the possibility that X=u is postulated to be equal to μ_z(u).

Referring to FIG. **22**, the steps required for DOC calculation for a pattern recognition approach are illustrated and can be summarized as follows:

Obtain a fuzzy set representing the membership **162** of the unknown pattern to all the possible classes. Rearrange the fuzzy set in descending order such that the first entry of the set represents the class with maximum membership. To obtain a possibility distribution **164**, normalize the fuzzy set

with respect to the maximum membership so that the maximum becomes equal to one. The mass function **166** for a nested body of evidence is calculated via Equation 29.

DOC **168** associated with each class is then calculated via Equation 21.

Active Perception in Sensor Fusion

In this section the active perception approach which performs the sensor fusion at feature level is explained. Let $F = \{F_1, \ldots, F_n\}$ be a set of n features extracted from the data obtained from m sensors to perform classification over the frame of discernment Θ having c atomic propositions. A total of n evidence can be generated using the n available features. Each evidence is represented as set of mass functions calculated from the fuzzy classifier output using the procedure explained in the section titled "Calculation of Mass Function". The evidence E_i is generated based on the ith feature by performing fuzzy classification using F_i, only. The evidence E_i obtained from the ith feature and evidence E_j obtained from the jth feature are combined using Dempster's rule of combination. For two body of evidence, represented as mass functions m_1 and m_2, the combined body of evidence, $m_{1,2}$, is obtained using the Dempster's rule of combination as

$$m_{1,2}(A) = \frac{\displaystyle\sum_{B_i \cap C_j = A} m_1(B_i) m_2(C_j)}{1 - K} \quad \forall\, A \in \Theta,\, A \neq \varnothing, \tag{30}$$

G. Shafer, A Mathematical Theory of Evidence, Princeton University Press, New Jersey, 1976.
where K is calculated by,

$$K = \sum_{B_i \cap C_j = \varnothing} m_1(B_i) m_2(C_j). \tag{31}$$

For active perception, F_i, and F_j, could be obtained from a single sensor data or from multiple sensor data to provide a combined body of evidence. Once a combined body of evidence is obtained, DOC associated with any subset of 2^{Θ} can be calculated using Equation 21.

The body of evidence $E_{1, \ldots, n}$ obtained by pooling n evidence is independent of the order in which pooling is performed. Therefore, the DOC associated with $E_{1, \ldots, n}$ is also independent of the evidence pooling order. However, the DOC trajectories are dependent on the order in which the pooling of evidence is performed. The DOC trajectories represent a set of loci on a two-dimensional plane whose axes are DOC and feature number. Let all the available features be ordered in a sequence. The DOC trajectory for the kth ordered feature F_k can be written as

$$\vec{t}(k) = k\vec{f} + a_k\vec{D}, \tag{32}$$

where f (with overhead vector arrow) and D (with overhead vector arrow) are unit vectors in the feature number and DOC axis, respectively. The sum of t (with overhead vector arrow) (k)+t (with overhead vector arrow) (k+1) is obtained as

$$\vec{t}(k) + \vec{t}(k+1) = (K+1)\vec{f} + (a_k \otimes a_{k+1})\vec{D}, \tag{33}$$

where $\otimes$ represents Dempster's rule of combination. Since, in general, $a_i \otimes a_j \neq a_i \otimes a_q$ for $j \neq q$, it is clear that the DOC trajectory is dependent on the order in which the various pieces of evidence are combined. Because evidence is obtained from the features, this implies that DOC is depen-

dent on the feature ordering. FIG. **23** illustrates an example of DOC trajectories when four pieces of evidence **163a**, **163b**, **163c** and **163d** are combined in three different orders **167a**, **167b** and **167c**. The four evidence expressed as mass functions are given in Table A

Evidence	Mass Functions
ϵ_1	$m_1(A) = 0.250\ m_1(ABC) = 0.750$
ϵ_2	$m_2(C) = 0.222\ m_2(AC) = 0.333\ m_2(ABC) = 0.444$
ϵ_3	$m_3(A) = 0.474\ m_3(AB) = 0.474\ m_3(ABC) = 0.032$
ϵ_4	$m_4(AB) = 1.000$

For supervised classification approaches, the a priori information about the classes is available in the form of a training data set. Using the training data set, the distinguishability power of each feature can be determined. Thus, it is a reasonable assumption that the knowledge base contains information about the distinguishability of features of each object as well as the time necessary to measure the features. It is generally true that the time required to derive a set of mass functions differs widely from one feature class to another, as much as from one sensor to another similar device. In order to achieve a reliable classification in the minimum amount of time, the features should be aligned in an optimal order such that features that require less processing time and provide greater distinguishability between classes should be first in the feature-ordering scheme. Assuming that an ordered feature set has been obtained, fuzzy classification is performed using one feature at a time from the ordered feature set. Each classification result based on a feature is converted into a body of evidence. Thus, for each feature, the classifier provides a piece of evidence. To determine the degree of perception achieved based on the latest evidence and all the previous evidence, DOC associated with the combined body of evidence is calculated. The total evidence is aggregated until the required DOC is achieved. The process of fuzzy classification is stopped as soon as enough evidence is obtained to achieve a pre-specified DOC. Thus, the active perception scheme controls the information-gathering process and uses that much information that is sufficient for the task at hand. FIG. **24** illustrates the active perception approach for a multisensory environment.

Referring to FIG. **24**, the active perception procedure **170** for defect classification is shown. The knowledge base **172**, represents the database including the optimal feature ordering and the training data set for the fuzzy classifier. The active perception procedure is generic in the sense that it can be applied in a multisensory **174** environment to perform sensor fusion at the feature level or on only the features extracted from a single sensor **171**. Features are extracted **176** and a fuzzy classification **178** is performed. A DOC is calculated **173** and a decision **177** is made on whether DOC threshold has been reached. If DOC threshold has not been reached an additional feature is considered. Once DOC threshold has been reached or total features evaluated indicating defect classification the process is stopped. To obtain the optimal order of the available features, the processing time for classification and the distinguishability for each feature should be evaluated. These evaluations can be performed as an off-line learning process, using the training data set. The feature-ordering scheme developed for active perception will be discussed in the section titled "Off-Line Learning". Feature ordering considers features from all available sensors, thus, fusing information from various sensors at feature level. An optimal feature ordering is

performed for each pair of classes. Let there be c number of classes that need to be classified. The total number of ordered feature sets required is $c(c-1)/2$. An ordered feature set, F_{ij} represents the feature order that maximizes distinguishability between the ith and the jth classes, while keeping the processing time low. During the active perception procedure, the DOCs for all possible classes are calculated based on the evidence provided by the current features and all previous ones. If the highest DOC value is less than the prespecified threshold, the next feature is selected so that it maximizes the distinguishability between the class with the highest DOC and the one with the second highest DOC. Thus, feature ordering for an unknown object is dynamically modified on-line during the active perception process.

To start the active perception procedure, the pairwise ordered feature sets cannot be used since all the classes have an equal chance of occurring. Therefore, another feature ordering that considers the distinguishability power of a feature with respect to all the classes and its processing time is also determined. The feature out of all the available features, which is optimum in terms of distinguishability with respect to all the classes and processing time, is selected as the first feature to start the active perception processes. This feature is called the first feature. The procedure to determine the first feature will be explained in the section titled "Off-Line Learning".

Distinguishability Measure

For the active perception scheme, the features need to be ordered on the basis of their ability to distinguish between various classes. Distinguishability measure quantifies a feature's ability to differentiate between various classes by finding the area of the region in which the two classes overlap. The smaller the area, the higher the ability of the feature to distinguish between the classes.

Suppose there are two classes, w_1 and w_2, that need to be classified based on a feature A. Let there be a training data set that includes N_1 samples belonging to w_1 and N_2 samples belonging to w_2. Assuming Gaussian distribution for the training data belonging to each class (a valid assumption for a large training data set), the mixture probability density function for feature A, can be written as

$$p(z) = \frac{P_1}{\sqrt{2\pi}\,\sigma_1}\exp\left(-\frac{(z-\mu_1)^2}{2\sigma_1^{\ 2}}\right) + \frac{P_2}{\sqrt{2\pi}\,\sigma_2}\exp\left(-\frac{(z-\mu_2)^2}{2\sigma_2^{\ 2}}\right), \quad (34)$$

where μ_1 is the mean of w_1 training data set, μ_2 is the mean of w_2 training data set, σ_1 is the standard deviation about μ_1, σ_2 is the standard deviation about μ_2, and P_1 and P are the a priori probabilities of the two classes. FIG. **25** illustrates one such mixture probability density function for a feature.

Referring to FIG. **25**, the shaded region **182** is the region for feature A, in which the two classes, w_1 and w_2 overlap. Let T **184** be a feature A value such that all the data points having feature A values less than T are considered belonging to class w_1 and all the data points having feature A values greater than or equal to T are considered belonging to class w_2. The probability of erroneously classifying w_1 data point as w_2 data point using feature A is

$$E_A^{w_1}(T) = \int_{-\infty}^{T} \frac{1}{\sqrt{2\pi}\,\sigma_2}\exp\left(-\frac{(z-\mu_2)^2}{2\sigma_2^{\ 2}}\right)dz. \quad (35)$$

Similarly, the probability of classifying a w_2 data point as a w_1 data point, using feature A is

$$E_{\mathcal{A}}^{w_1}(T) = \int_T^\infty \frac{1}{\sqrt{2\pi}\,\sigma_1} \exp\left(-\frac{(z-\mu_1)^2}{2\sigma_1^2}\right) dz. \tag{36}$$

Therefore, the overall probability of error, for feature A is

$$E_A(T) = P_2 E_A^{w_1}(T) + P_1 E_A^{w_2}(T). \tag{37}$$

Referring now to FIG. **25**, the shaded region **182** graphically represents Equation 37. E_A (T) can be considered as a distinguishability measure for feature A to differentiate between classes w_1, and w_2. Since both classes have an equal chance of occurring, the a priori probabilities are $P_1 = P_2 = 0.5$ and can be neglected in Equation 37 for comparison purposes. Thus, the distinguishability measure of feature A for classes w_1 and w_2 is

$$d_A^{w_1,w_2} = E_A^{w_1}(T) + E_A^{w_2}(T), \tag{38}$$

where $E_A^{w_1}$ (T) is calculated using Equation 35 and $E_A^{w_2}$ (T) is calculated using Equation 36

FIG. **26** illustrates the feature distinguishability measure graphically. The mean value of a feature for a particular class **192** is shown. A small value of distinguishability measure is shown as shaded area **194** illustrating an example of a "good" feature, while a large value of distinguishability measure is shown as shaded area **196** illustrating an example of a "bad" feature. To calculate $d_A^{w_1,w_2}$, T needs to be determined. The value of T is determined such that E_A (T) is minimal. This is done by differentiating E_A (T) with respect to T and equating the result to zero. Thus, by Liebnitz's rule, we get

$$\frac{1}{\sigma_1}\exp\left(-\frac{(T-\mu_1)^2}{2\sigma_1^2}\right) = \frac{1}{\sigma_2}\exp\left(-\frac{(T-\mu_2)^2}{2\sigma_2^2}\right). \tag{39}$$

Taking the natural logarithm of Equation 39 and simplifying gives the quadratic equation

$$AT^2 + BT + C = 0, \tag{40}$$

where

$A = \sigma_1^2 - \sigma_2^2$

$B = 2(\mu_1\sigma_2^2 - \mu_2\sigma_1^2)$

$C = \sigma_1^2\mu_2^2 - \sigma_2^2\mu_1^2 + 2\sigma_1^2\sigma_2^2 \ln(\sigma_2/\sigma_1)$

Of the two possible solutions for T, the value is selected such that one of the following conditions is satisfied. The conditions are

$\mu_1 < T \leq \mu_2$

$\mu_1 \leq T < \mu_2$

$\mu_1 < T \leq \mu_1$

$\mu_1 \leq T < \mu_1$.

If the variances are equal, $\sigma^2 = \sigma_1^2 = \sigma_2^2$, a single solution is obtained for T that is equal to the average of the means. If the means are equal, $\mu = \mu_1 = \mu_2$, all the conditions for the selection of a single T are violated. When $\sigma_1^2 \neq \sigma_2^2$ and $\mu = \mu_1 = \mu_2$, T has two valid solutions, T_1 and T_2. The distinguishability measure, $d_B^{w_1,w_2}$ of feature B for classes w_1 and w_2 with two valid Ts is calculated as

$$d_B^{w_1,w_2} = \frac{1}{\sqrt{2\pi}}\int_{T_1}^{T_2}\left[\frac{1}{\sigma_1}\exp\left(-\frac{(z-\mu_1)^2}{2\sigma_1^2}\right) + \frac{1}{\sigma_2}\exp\left(-\frac{(z-\mu_2)^2}{2\sigma_2^2}\right)\right] dz. \tag{41}$$

where $T_1 < T_2$. When $\sigma_1^2 = \sigma_2^2$ and $\mu_1 = \mu_2$, i.e., the two distributions are exactly the same, Equation 40 is undercon-

strained. For such a case, the distinguishability measure, $d_B^{w_1,w_2}$, of feature B for classes w_1 and w_2 is equal to 2.0, calculated by using Equation 41 with $T_1 = -\infty$ and $T_2 = +\infty$.

Learning

Learning is the process of acquiring knowledge. In a pattern recognition paradigm, learning is often used as a synonym for training the classification stage. R. Gonzalez and R. Woods, Digital Image Processing, Addison-Wesley Publishing Company, Reading, Mass., 1992. This learning is achieved using the training data set. In an artificial neural network paradigm, learning is defined as a process accomplished by incorporating past experiences into the interconnection weights. The learning accomplished by using the a priori information (training data set) is also called off-line learning. Learning can also be regarded as an ongoing process. Whenever new information supporting a prior knowledge is acquired, it is plausible to say the learning has been accomplished. I. Kim, A Hybrid Analytical/Intelligent Methodology for Sensor Fusion, Doctoral Thesis, Georgia Institute of Technology, December, 1992. This type of learning is called on-line learning.

For FINE inspection, learning is accomplished both as an off-line process and as an on-line process. The off-line learning is achieved by incorporating the a priori knowledge about the classes in terms of feature ordering for active perception. The on-line learning process fine tunes the feature ordering by aggregating the feature effectiveness calculated while performing the pattern recognition of unknown objects.

Off-Line Learning

Off-line learning is accomplished by performing the feature ordering for the active perception scheme. The training data set, which provides the a priori information about the various classes of interest, is used for the off-line learning process.

The feature ordering is performed using the distinguishability measure, previously defined in the section titled "Distinguishability Measure", and the processing time required for each feature extraction. The processing time for a feature can be determined in terms of the central processing unit (CPU) time of a computer, floating point operations per second (flops), or clock time.

Let there be N total features that are used to classify c number of classes. As mentioned previously in the section titled "Active Perception in Sensor Fusion" the total number of ordered feature sets required for c classes is c(c−1)/2. Let F_{ij}, i=1, . . . , c, j=i+1, . . . , c, ≠j, represent the ordered feature set for the ith and the jth class pair. Let τ_k represent the processing time required to extract the kth feature, f_k, where k=1, . . . , N. A cost function for each feature is evaluated by considering its processing time and the distinguishability measure for classifying a class pair. Let ξ_k^{ij} be the cost function of the kth feature for the ith and the jth class pair, where k=1, . . . , N, i=1, . . . , c, j=i+1, . . . , c, i≠j. The cost function of the kth feature for class i and j is calculated as

$$\xi_k^{ij} = w_1 \hat{d}_{fk}^{ij} + w_2 \hat{\tau}_k, \tag{42}$$

where w_1, w_2 are weighting constants, selected such that $w_1 + w_2 = 1$. $\hat{d}_{fk}^{ij}$ represents the normalized distinguishability measure of the kth feature f_k for the ith and jth class and $\hat{\tau}_k$ represents the normalized processing time for the kth feature. d_{fk}^{ij} is calculated as

$$\hat{d}_{jk}^{i,j} = \frac{d_{jk}^{i,j}}{\max_k\{d_{jk}^{i,j}\}}, \tag{43}$$

where d_{jk}^{ij} is the distinguishability measure of the kth feature f_k for the ith and the jth class and is calculated using Equation 38. The normalized processing time for the kth feature τ_k, is calculated as

$$\hat{\tau}_k = \frac{\tau_k}{\max_k\{\tau_k\}}. \tag{44}$$

The cost function ξ_k^{ij} is calculated for $c(c-1)/2$ number of class pairs and for all the available features. These cost functions can be represented as a matrix Ψ given as

$$\Psi = \begin{bmatrix} \zeta_1^{12} & \zeta_1^{13} & \cdots & \zeta_1^{1c} & \zeta_1^{23} & \cdots & \zeta_1^{2c} & \cdots & \zeta_1^{(c-1)c} \\ \zeta_2^{12} & \zeta_2^{13} & \cdots & \zeta_2^{1c} & \zeta_2^{23} & \cdots & \zeta_2^{2c} & \cdots & \zeta_2^{(c-1)c} \\ \vdots & & & & & \ddots & & & \vdots \\ \zeta_N^{12} & \zeta_N^{13} & \cdots & \zeta_N^{1c} & \zeta_N^{23} & \cdots & \zeta_N^{2c} & \cdots & \zeta_N^{(c-1)c} \end{bmatrix}. \tag{45}$$

The feature ordering F_{ij} for the ith and the jth class pair is obtained by sorting the column of Ψ, which represents cost functions for the ith and the jth class pair in ascending order. Thus, the first entry of the feature ordering F_{ij} for the ith and the jth class pair is the feature f_q which satisfies the following relation:

$$f_q = \min_k\{\zeta_k^{ij}\} \quad \text{for } k = 1, \ldots, N. \tag{46}$$

To begin the active perception procedure, the first feature is required. As mentioned previously in the section titled "Active Perception in Sensor Fusion", the pairwise ordered feature sets cannot be used to initiate the active perception procedure since all the classes have an equal chance of occurring. The first feature is determined by considering its distinguishability power for all the possible class pairs and its processing time. The first feature, f_{1st}, is the feature whose cost function ξ_1^{st}, satisfies

$$\zeta_{1st} = \min_k\left\{\sum_{i=1, j=i+1}^{c} \zeta_k^{ij}\right\}, k = 1, \ldots, N, \tag{47}$$

where ξ_k^{ij} is the cost function calculated using Equation 42 with weighting factors $w_1 = w_2 = 0.5$. N is the total number of available features and c is the total number of classes.

On-line Learning

On-line learning has been incorporated into the FINE inspection for adapting the active perception algorithm to the system changes by fine tuning the feature ordering obtained from the off-line learning process. A measure has been defined to monitor the system changes in terms of feature utilization. This measure is called the effectiveness of a feature.

The off-line learning process uses the training data set to determine the ordered feature sets. For defect classification, the training data set is gathered so as to provide examples of solder joints belonging to various defect classes. It is desirable that the training data set include all the possible patterns that belong to a single defect class in order to determine its

correct cluster type in the feature space. In practice, the solder joint defects that are generated by the system (resulting from malfunctions or drift in control parameters) may cover a limited range of the expected feature range. Therefore, a feature that is considered bad on the basis of distinguishability measure (calculated using the training data set) may perform better under the current operating conditions of the system. Referring now to FIG. 27, a linearly misaligned surface-mounted integrated circuit (IC) has its leads 202 shifted to one side with reference to the solder pads 204 underneath. Consider the offset 206 between a solder pad centerline and an IC's lead centerline as a feature. For a 50 mil (mil is a unit used in the electronics manufacturing industry. 1 mil=1×10^{-3} inch.) pitch IC, this feature may have values in the range of 0.25 mm to 1.25 mm.

However, the system may generate the linear misalignment defects with centerline offsets in the range of 0.25 mm to 0.50 mm. Thus, by monitoring the current state of system operation, the ordered feature sets may be rearranged such that the active perception process is adapted to the system's current operational state.

A learning procedure has been developed by on-line monitoring of the effectiveness of the features used by the active perception process for an unknown pattern. The effectiveness of a feature in distinguishing between two classes is determined on-line from the fuzzy partition of an unknown pattern. The effectiveness, n_k^{ij}, of the kth feature in distinguishing the ith and the jth classes is defined as

$$\eta_k^{i,j} = |\mu_{ik}(x) - \mu_{jk}(x)|, \tag{48}$$

where $|\cdot|$ represents absolute operation, μhd ik(x)is the jth class membership of the unknown pattern x, and $\mu_{jk}(x)$ is the jth class membership of x.

The effectiveness of all the features for all the class pairs, which are employed during the active perception, is determined for a finite number of classifications. The effectiveness obtained for all the classifications is summed together and normalized for each class pair such that the maximum effectiveness becomes equal to 1.0. A new cost function ξ_k^{ij} of the kth feature for the ith and the jth class pair is calculated as

$$\xi_k^{i,j} = w_1\hat{\eta}_k^{i,j} + \frac{w_2}{\hat{\tau}_k}, \tag{49}$$

where η_k^{ij}, represents the normalized effectiveness of the kth feature for the ith and the jth class pair, τ_k is the normalized processing time for the kth feature. w_1 and w_2 are weighting factors for feature effectiveness and its processing time, respectively. The weighting factors are selected such that $w_1 + w_2 = 1.0$. The cost function ξ of all the features and for all the class pairs are represented as a matrix Γ, given as

$$\Gamma = \begin{bmatrix} \xi_1^{12} & \xi_1^{13} & \cdots & \xi_1^{1c} & \xi_1^{23} & \cdots & \xi_1^{2c} & \cdots & \xi_1^{(c-1)c} \\ \xi_2^{12} & \xi_2^{13} & \cdots & \xi_2^{1c} & \xi_2^{23} & \cdots & \xi_2^{2c} & \cdots & \xi_2^{(c-1)c} \\ \vdots & & & & & \ddots & & & \vdots \\ \xi_N^{12} & \xi_N^{13} & \cdots & \xi_N^{1c} & \xi_N^{23} & \cdots & \xi_N^{2c} & \cdots & \xi_N^{(c-1)c} \end{bmatrix}, \tag{50}$$

where N is the total number of available features and c is the total number of classes. The feature ordering F_{ij} for the ith and the jth class pair is obtained by sorting the column of Γ, which represents cost functions for the ith and the jth class pair in descending order. Thus, the first entry of the feature

5,963,662

23

ordering F_{ij} for the ith and the jth class pair is the feature f_q which satisfies the following relation:

$$f_q = \max_k \{\xi_k^{i,j}\} \quad \text{for } k = 1, ..., N. \tag{51}$$

Linear Misalignment Test

At the FINE inspection station, the linear misalignment test is triggered only if the GROSS inspection station finds a possible linearly misaligned solder joint. The linear misalignment test at the FINE inspection confirms whether the solder joints under inspection are linearly misaligned or not. Since the IR detector is insensitive to the placement defects, only vision data i.e. two-dimensional 256 gray level images, is used for linear misalignment defect classification.

The shadow free higher resolution images of the probable defective solder joints are captured using a front diffuse illumination technique. FIG. 20 illustrates an image of a typical linear misalignment defect 151. The preprocessing technique called max scan, developed for GROSS inspection, can be applied to high resolution FINE inspection images, since the max scan is independent of the image resolution.

A max scan of the solder joints under test is calculated and compared with the max scan of good solder joints. Since the images are of high resolution, the max scan can handle noise more effectively. The noise is sometimes generated because of printed letters and traces in the processing window of max scan. A linguistic labels based fuzzy classifier is used for linear misalignment defect classification. The fuzzy classifier was explained previously in the section titled Defect Identification using Fuzzy Relations and Linguistic Variables.

Excess Solder Mass Test

The excess solder mass test is triggered at the FINE inspection station, if the IR GROSS inspection detects a solder joint with more solder mass than a good solder joint. The objective of this test module is to inspect the probable defective solder joint and to classify it into bridging, ball, or excess solder defect classes. In case of a false alarm at the GROSS inspection station, this test module should classify the solder joint as good.

This classification module uses the active perception approach to fuse vision and IR data at feature level. High resolution images of the probable defective solder joints are captured using a CCD camera. The IR thermal signature of these solder joints, captured at the GROSS inspection station, are also called upon for detailed investigation. Features are extracted from the image as well as the IR thermal signatures of the joint under test. The complete feature set available for the active perception consists of 15 vision based features and 19 IR thermal signature based features. The output of the test is the class declaration of the solder joint under test with the associated degree of certainty.

Insufficient Solder Mass Test

The insufficient solder mass test is triggered at the FINE inspection station, if the IR GROSS inspection detects a solder joint with less solder mass than a good solder joint. The objective of this test module is to inspect the probable defective solder joint and to classify it into void, insufficient, or no solder defect classes. In case of a false alarm at the GROSS inspection station, this test module should classify the solder joint as good.

This classification module uses the active perception approach to fuse vision and IR data at feature level. High resolution images of the probable defective solder joints are

24

captured using a CCD camera. The IR thermal signature of these solder joints, captured at the GROSS inspection station, are also called upon for detailed investigation. Features are extracted from the image as well as the IR thermal signatures of the joint under test. The complete feature set available for the active perception consists of 15 vision based features and 19 IR thermal signature based features. The output of the test is the class declaration of the solder joint under test with the associated degree of certainty

Menu Driven User Interface

This section details the software developed for the prototype operation and user interface. To make the prototype user-friendly, efforts were devoted to the development of a user-friendly interface which can be used as the basic platform for integrating various processing, recognition and control algorithms. The development of the user-interface facilitated the integration of the overall methodology for the GROSS inspection and FINE inspection.

In designing a user-friendly interface for the prototype, consideration was given to make it as simple and as self explanatory as possible. The interface developed is menu driven. When a user wishes to interact with the experimental setup, he/she is offered a list of options to select from. The menus are nested in such a way that if any menu option requires a prerequisite action, the option could not be selected until the prerequisite action has been performed. If the user selects such an option, a message directing the user to the prerequisite action is displayed on the screen. The X-Y table motion control, laser firing and image capture procedures have been embedded in the menu driven options such that they are transparent to the user. If a selected option requires X-Y table motion and image capture, it is performed automatically. The training phase for a new PCB for inspection has been developed such that it reduces to simple mouse driven and/or arrow keys operation. The software for the interface has been developed using C computer language. The programming has been done in a modular fashion so that adding new menus or new options to existing menu do not require any modification of the existing menus. FIG. 28 illustrates a menu screen developed for the prototype.

Results

A set of five GVC Ethernet cards were purchased and a number of defects were created at the U.S Army Missile Command soldering facility at Huntsville, Alabama. The algorithms developed for GROSS inspection and FINE inspection were tested on these PCBs.

GROSS Inspection Results

The perceptron classifier for the component presence test gave 100% correct classification results. The classifier is very reliable and robust to shadow side window placement and the angle of illumination. The linear misalignment and angular misalignment test did not miss any existing defects, but for some PCBs they had a false alarm of 3% to 4%. The false alarms were created because of the printed letters and traces in the processing window. These printed letters and traces appear as bright spots in the processing windows. To avoid the false alarms, the processing windows need to be defined carefully. This requirement makes these test procedures sensitive to the window location. The processing time for the vision GROSS inspection, depending upon the number of processing windows and their sizes ranging from 0.7 seconds to 1.5 seconds.

The perceptron classifier for the IR GROSS inspection detected all the defective solder joints and classified them correctly into excess solder mass category or insufficient solder mass category. The IR GROSS inspection had a false alarm of 2%. The false alarms were created because of the

high sensitivity of InSb sensor to the surface profile of the solder joint. If the surface of the solder joint is contaminated with dust particles or flux, the InSb sensor may not detect any signal at all. The MCT sensor is not sensitive to these variations.

FINE Inspection Results

The linear misalignment test module at the FINE inspection station classified all the linearly misaligned solder joints correctly. The satisfactory performance of this module illustrates that max scan is independent of the image resolution and can be effectively applied at various resolution levels.

The excess solder mass test module was tested using 52 solder joints belonging to good, excess solder, bridging, and ball classes. The DOC threshold was set to 0.90. The active perception approach to classification misclassified one excess solder joint as bridging defect. The remaining 51 solder joints were classified correctly. The application of active perception allowed the classification of defects to be performed using a subset of the 38 feature set. FIG. 29 illustrates the DOC trajectories 212 obtained for an excess solder defect classification using the active perception approach. Note that the classification is performed using only six features 214 with a DOC of 0.915 216.

FIG. 30 illustrates DOC trajectories 212 obtained for a bridging defect classification. For this case, only four features 218 were used and the associated DOC is 0.920 222.

FIG. 31 illustrates the DOC trajectories 212 obtained for a solder ball defect classification.

This test module also classified the good solder joints correctly. FIG. 32 illustrates the DOC trajectories 212 obtained for a good solder joint classification.

The active perception scheme aggregates the evidence obtained from each feature until the specified degree of certainty is obtained. This means that for borderline defect cases between defect classes, more features are used as compared to the typical defects. FIG. 33 illustrates the DOC trajectories 212 obtained for a bridging defect using 17 features 224 out of an available 38.

The classification of 52 solder joints, by the excess solder mass test module, was performed using 139 features which is 7% of the total available features.

The insufficient solder mass test module was tested using 41 solder joints belonging to good, insufficient, and no solder classes. The DOC threshold was set to 0.90. The module gave 100% results. The 41 solder joints were classified using 78 features which is 5% of the total available features.

FIG. 34 and FIG. 35 show the DOC trajectories 212 obtained by the insufficient solder mass test, for an insufficient solder defect and a good solder joint, respectively.

The FINE inspection results show that the active perception scheme using sensor fusion at feature level not only performs the classification with a fewer number of features (which implies less processing time), but also provides an index of confidence associated with the classification.

It is to be understood that the foregoing is descriptive of an illustrative, preferred embodiment of the invention. Numerous variations or changes may occur to those skilled in the art without departure from the spirit and scope of the invention.

Wherein the following is claimed:

1. A system for detecting solder joint defects on surface mount components on a printed wiring board, comprising:
    a machine vision sensor that collects visual inspection information pertaining to a surface mount component, said visual inspection information used to develop programmed rectangular windows from which sub-

images of said surface mount component are developed, said sub-images used to develop a one-dimensional vector corresponding to placement of said surface mount component on the printed wiring board, said one-dimensional vector having peaks and valleys, wherein said peaks represent solder joints and said valleys represent a substrate upon which said surface mount component is moumted;
    at least one infrared sensor that collects thermal signature inspection information pertaining to a surface mount component; and
    a processing means for processing said visual inspection information and said thermal signature inspection information in order to detect and classify said solder joint defects on said surface mount components on said printed wiring board, said processing means including a means for processing said one-dimensional vector corresponding to the placement of said surface mount component on the printed wiring board using a morphological filter, said processing means also including means for fusing the data from a plurality of said infrared sensors using data level sensor fusion to obtain emissivity independent thermal signatures of solder joints.

2. The system according to claim 1, wherein said processing means comprises a combinational logic circuit configured to perform said processing.

3. The system according to claim 1, wherein said processing means comprises a neural network configured to perform said processing.

4. The system according to claim 1, further comprising:
    an additional infrared sensor; and
    means for combining said thermal signature inspection information from said infrared sensor and said additional infrared sensor.

5. The system according to claim 4, wherein said infrared sensor and said additional infrared sensor provide an emissivity independent thermal signature.

6. A computer readable medium having a program for detecting solder joint defects on surface mount components on a printed wiring board, the program comprising:
    means for receiving visual inspection information from a machine vision sensor, said visual inspection information used to develop programmed rectangular windows from which sub-images of said surface mount component are developed, said sub-images used to develop a one-dimensional vector corresponding to placement of said surface mount component on the printed wiring board, said one-dimensional vector having peaks and valleys, wherein said peaks represent solder joints amid said valleys represent a substrate upon which said surface mount component is mounted;
    means for receiving thermal signature inspection information from at least one infrared sensor; and
    means for processing said visual inspection information and said thermal signature inspection information resulting in the inspection of surface mount component solder joints on said surface mount components on said printed wiring board, said processing means including a means for processing said one-dimensional vector corresponding to the placement of said surface mount component on the printed wiring board using a morphological filter, said processing means also including means for fusing the data from a plurality of said infrared sensors using data level sensor fusion to obtain emissivity independent thermal signatures of solder joints.

7. The program according to claim **6**, wherein said processing means comprises a combinational logic circuit configured to perform said processing.

8. The program according to claim **6**, wherein said processing means comprises a neural network configured to perform said processing.

9. The program according to claim **6**, further comprising:

means for receiving an additional thermal signature information from an additional infrared sensor; and

means for combining said thermal signature inspection information from said infrared sensor and said additional infrared sensor.

10. A system for combining and processing the complimentary nature of visual inspection information and thermal signature inspection information to increase the degree of probability of detecting a solder defect in an object, comprising:

a computer system which processes said inspection information, said inspection information including visual inspection information and thermal signature inspection information, said visual inspection information used to develop programmed rectangular windows from which sub-images of said surface mount component are developed, said sub-images used to develop a one-dimensional vector corresponding to placement of a surface mount component on a printed wiring board, said one-dimensional vector having peaks and valleys, wherein said peaks represent solder joints and said valleys represent a substrate upon which said surface mount component is mounted and said thermal signature inspection information obtained by fusing data from a plurality of said infrared sensors using data level sensor fusion to obtain enissivity independent thermal signatures of solder joints; and

a statistical sampling means for detecting said solder defect in said object, said statistical sampling means including a morphological filter for processing said one-dimensional vector.

11. The system of claim **10**, further comprising a means for classifying said visual inspection information for comparison against a known good specimen.

12. The system of claim **10**, further comprising a means for classifying said thermal signature inspection information for comparison against a known good specimen.

13. A method for detecting solder joint defects on surface mount components on a printed wiring board, comprising the steps of:

collecting visual inspection information and thermal signature inspection information, said visual inspection information used to develop programmed rectangular windows from which sub-images of said surface mount component are developed, said sub-images used to develop a one-dimensional vector corresponding to placement of said surface mount component on the printed wiring board, said one-dimensional vector having peaks and valleys, wherein said peaks represent solder points and said valleys represent a substrate upon which said surface mount component is mounted, said thermal signature inspection information obtained by fusing data from a plurality of infrared sensors using

data level sensor fusion to obtain emissivity independent thermal signatures of solder joints; and

processing said visual inspection information and said thermal signature inspection information resulting in the inspection of surface mount component solder joints on said surface mount components on said printed wiring board, said processing step including the step of processing said one-dimensional vector corresponding to the placement of said surface mount component on the printed wiring board using a morphological filter, said processing step also including the step of fusing the data from a plurality of said infrared sensors using data level sensor fusion to obtain emissivity independent thermal signatures of solder points.

14. A system for detecting solder joint defects on surface mount components on a printed wiring board, comprising:

a machine vision sensor that collects visual inspection information pertaining to a surface mount component, said visual inspection information used to develop programmed rectangular windows from which sub-images of said surface mount component are developed, said sub-images used to develop a one-dimensional vector corresponding to placement of said surface mount component on the printed wiring board, said one-dimensional vector having peaks and valleys, wherein said peaks represent solder joints and said valleys represent a substrate upon which said surface mount component is mounted;

at least one infrared sensor that collects thermal signature inspection information pertaining to a surface mount component; and

logic configured to process said visual inspection information and said thermal signature inspection information in order to detect and classify said solder joint defects on said surface mount components on said printed wiring board, said processing means including means for processing said one-dimensional vector corresponding to the placement of said surface mount component on the printed wiring board using a morphological filter, said logic also configured to fuse the data from a plurality of said infrared sensors using data level sensor fusion to obtain emissivity independent thermal signatures of solder joints.

15. The system according to claim **14**, wherein said logic comprises a combinational logic circuit configured to perform said processing.

16. The system according to claim **14**, wherein said logic comprises a neural network configured to perform said processing.

17. The system according to claim **14**, further comprising:

an additional infrared sensor; and

logic configured to combine said thermal signature inspection information from said infrared sensor and said additional infrared sensor.

18. The system according to claim **17**, wherein said infrared sensor and said additional infrared sensor provide an emissivity independent thermal signature.

* * * * *

UNITED STATES PATENT AND TRADEMARK OFFICE
CERTIFICATE OF CORRECTION

PATENT NO.   : 5,963,662   Page 1 of 4
DATED   : October 5, 1999
INVENTOR(S) : Vachtsevanos et al.

It is certified that error appears in the above-identified patent and that said Letters Patent is hereby corrected as shown below:

Column 3,
Line 61, after "temperatures", delete -- and --.

Column 5,
Line 38, before "GROSS Inspection Software", insert a blank line.
Line 59, before "Vision Based GROSS Inspection", insert a blank line.

Column 7,
Line 31, after "element," delete "(symbol bigodot0", and insert -- bigdotO --.
Line 45, Equation 6, after "$\neq$", change

"ϕ", to -- $\varnothing$ --.

Column 8,
Line 7, after "be", delete "$(X_{pl},\ Y_{pl})$", and insert -- $(x_{pl},\ y_{pl},)$ --.
Line 7, after "and", delete "$(X_{p2},\ Y_{p2})$", and insert -- $(x_{p2},\ Y_{p2})$ --.
Line 28, before "Defect Identification using Fuzzy Relations and Linguistic," insert a blank line.
Line 46, after "relation", delete "__", and insert -- $\mathfrak{R}$ --
Line 61, after "membership of", delete "u", and insert -- v --.

Column 9,
Line 11, delete "corresponding$_{13}$", and insert -- corresponding γ --.
Line 12, delete "membership__", and insert -- membershipφ --.
Line 14, Equation 12, delete "$\Phi = \gamma \circ R$", and insert -- $\varphi = \gamma \circ \mathfrak{R}$ --.
Line 37, after "relation", delete "R", and insert
" $\mathfrak{R}$ ".

Line 39, before "IR Based GROSS Inspection", insert a blank line.
Line 64, before "Emissivity Dependent Thermal Signature", insert a blank line.

Column 10,
Line 42, before "Fusion of IR Detectors", insert a blank line.

It is certified that error appears in the above-identified patent and that said Letters Patent is hereby corrected as shown below:

Column 12,
Line 7, before "GROSS Inspection using Thermal Signatures", insert a blank line.
Line 41, before "FINE Inspection Software", insert a blank line.

Column 13,
Line 29, before "Active Perception", insert a blank line.
Line 59, before "Degree of Certainty", insert a blank line.
Line 60, after "discernment", delete " Θ ", and insert -- θ --.
Line 66, after "over", delete " Θ ", and insert -- θ --.

Column 14,
Line 1, after "over", delete "Θ ", and insert -- θ --.
Line 1, after "Bel:", delete "$2^{\Theta} \to$ [0,1]", and insert -- $2^{\theta} \to$ [0,1] --.
Equation 22, delete and insert

$$\text{"}Bel(A) = \sum_{B \subseteq A} m(B) \vee A \subseteq \Theta \text{",}$$

$$-- Bel(A) = \sum_{B \subseteq A} m(B) \vee A \subseteq \theta --.$$

Line 17, after "rest of", delete " Θ ", and insert -- θ --.
Line 24, after "subsets of", delete "2^{Θ}" and insert -- 2^{θ} --.
Line 25, after "subset of", delete " Θ ", and insert -- θ --.
Line 28, before "Calculation of Mass Function", insert a blank line.
Equation 24, delete " $\pi(A \cup B) = \max[\pi(A), \pi(B)] \forall A, BA2^{F}$ ",

$$\text{and insert } -- \pi(A \cup B) = \max[\pi(A), \pi(B)] \forall A, B \in 2^{F} --.$$

Line 61, after "discernment", delete " Θ = ", and insert -- θ = --.
Line 66, after "all", delete " $x_i \in \Theta$ ", and insert -- $x_i \in \theta$ --.

Line 67, after "defined on", delete "2^{Θ}" and insert -- 2^{θ} --.

UNITED STATES PATENT AND TRADEMARK OFFICE
CERTIFICATE OF CORRECTION

PATENT NO.   : 5,963,662   Page 3 of 4
DATED   : October 5, 1999
INVENTOR(S)   : Vachtsevanos et al.

It is certified that error appears in the above-identified patent and that said Letters Patent is hereby corrected as shown below:

Column 15,
Line 2, before "152", delete " Θ = ", and insert -- θ = --.
Line 9, after "for all", delete " x $\varepsilon\Theta$ ", and insert -- $x\varepsilon$ θ --.
Equation 27, delete and insert

$$\text{``} Pl(A) = \sum_{A \cap B \neq 0} m(B) \forall A \subseteq \Theta \text{''},$$

$$-- Pl(A) = \sum_{A \cap B \neq 0} m(B) \forall A \subseteq \theta --.$$

Line 26, after "elements of", delete " Θ = ", and insert -- θ = --.

Column 16,
Line 6, before "Active Perception in Sensor Fusion", insert a blank line.
Line 11, after "discernment", delete " Θ = ", and insert -- θ = --.
Equation 30, delete

$$\text{``} m_{1,2}(A) = \frac{\sum_{B_i \cap C_j = A} m_1(B_i) m_2(C_j)}{1 - K} \forall A \in \Theta, A \neq 0 \text{''}, \text{ and}$$

insert

$$-- m_{1,2}(A) = \frac{\sum_{B_i \cap C_j = A} m_1(B_i) m_2(C_j)}{1 - K} \forall A \in \theta, A \neq 0 --.$$

Line 41, after "subset of", delete and insert "2^{Θ}", and insert -- 2^{θ} --.

Column 17,
Table A, line 3, after m₃(ABC)=", delete, "0.032", and insert -- 0.052 --.

Column 18,
Line 27, before "Distinguishability Measure", insert a blank line.

Column 19,
Line 44, delete " $B = 2(\mu_1 \sigma_2^{2-} \mu_2 \sigma_1^2$ ", and insert -- $B = 2(\mu_1 \sigma_2^2 - \mu_2 \sigma_1^2)$ --

Column 20,
Line 17, after "supporting a", change "prior", to -- priori --.

UNITED STATES PATENT AND TRADEMARK OFFICE
CERTIFICATE OF CORRECTION

PATENT NO.   : 5,963,662
DATED   : October 5, 1999
INVENTOR(S) : Vachtsevanos et al.

It is certified that error appears in the above-identified patent and that said Letters Patent is hereby corrected as shown below:

Column 21,
Line 54, before "On-Line Learning", insert a blank line.

Column 22,
Line 33, after "operation," delete " μ hd ik(x)", and insert -- μ_{ik} (x) --.

Column 23,
Line 34, before "Excess Solder Mass Test", insert a blank line.
Line 56, before "Insufficient Solder Mass Test", insert a blank line.

Column 24,
Line 9, after "certainty", insert -- . --.
Line 10, before "Menu Driven User Interface", insert a blank line.
Line 41, before "Results", insert a blank line.
Line 47, before "GROSS Inspection Results", insert a blank line.

Column 25,
Line 6, before "FINE Inspection Results", insert a blank line.

Column 26, claim 6,
Line 50, after "solder joints", delete "amid", and insert -- and --.

Column 28, claim 13,
Line 15, after "of solder", delete "points", and insert -- joints --.

Signed and Sealed this

Eighth Day of January, 2002

Attest:

JAMES E. ROGAN
Director of the United States Patent and Trademark Office

Attesting Officer